Eye-Safe UV Stand-off Raman Spectroscopy for Explosive Detection in the Field

Joshua Adam Carroll

Supervisor:
Assoc Prof. Esa Jaatinen

Associate Supervisor:
Dr. Emad Kiriakous

Submitted to the Science and Engineering Faculty, Queensland University of Technology, in fulfilment of the requirements for the degree of Master of Applied Science (Research)

January 16, 2015

Acknowledgements

I would firstly like to thank my supervisor, Esa Jaatinen, for all of his teaching and advice over the course of my undergraduate and master's degrees. Through his guidance I have achieved and learnt so much, which I will always be extremely grateful for.

I also would like to thank my associate supervisor, Emad Kiriakous, who continually looked out for me and provided his equipment for my experiments. The equipment he provided me with was key to completing my project and I am very thankful to him.

Thank you to Biju Cletus, who showed me how to operate all the of the equipment, and gave me a big helping hand in getting my project started. I really appreciate all the help you have given me over the past year.

To Matthew Shortell, I am extremely grateful for all the times in which you helped me solve a problem I was stuck on, and for often taking the time to share your wisdom and expertise with me.

I would also like to acknowledge Konstantin Momot, when I needed advice outside of my scope he was always happy to make time for me.

Thanks to all my colleagues at QUT for providing such a great community, especially the physics post graduates who helped to regularly replace stress with coffee and beer.

Finally I would like to thank my family, my partner, and her family for their continued support during my studies.

Abstract

The rising number of terrorist attacks that involve the use of explosives highlights the pressing need for rapid, accurate and safe detection methods to be developed that can be deployed in the field. Methods that are currently used for explosive detection suffer from limitations such as requiring long signal acquisition times, or the need for operators to be in close proximity to the potential hazard. Clearly a more preferable approach is to use a technique that is capable of detecting explosives from safe operator distances, over realistic timescales. Stand-off Raman spectroscopy is a method which can detect substances more than 100 m away in less than a second. In addition, as it is an optical technique it can achieve detection without making physical contact with a sample, reducing the risk of accidental detonation.

Detection of substances at distance using stand-off Raman spectroscopy often requires the use of high power lasers, since the operating range of the system is ultimately limited by the power of the light source used. Unfortunately, the use of accessible laser beams with high power densities creates significant practical problems in terms of operating the stand-off Raman system in the field, due to the risk of eye or skin injury to operators and bystanders. As a result of this safety concern, stand-off Raman spectroscopy is a relatively underutilised technique for explosives detection, despite being technically superior to alternative approaches.

In this thesis, the maximum laser power densities that the eye and skin can safely be exposed to, are evaluated for different wavelengths in order to identify spectral regions where both organs are more resilient to injury. This analysis shows that in both the ultraviolet and infrared regions of the spectrum, it is possible to use lasers without risk of injury that have powers between 2 to 4 orders of magnitude greater than in the visible and near infrared regions. Using the light and beam properties that are characteristic of typical 266 nm and 532 nm commercial lasers that radiate within these spectral windows, the maximum detection range is evaluated when the laser is used for stand-off Raman detection. The addition of the higher pulse energies that can be safely used in the UV, and the 16 fold increase in Raman signal due to scatterings dependence on wavelength, results

in a 131 times larger detection range for the eye-safe 266 nm system over an equivalent eye-safe 532 nm laser system. For the Raman system described here, this translates to a maximum range of 42 m for detecting Teflon with a 266 nm laser emitting a 100 mm diameter beam of 23 mJ nanosecond pulses. Results are also shown that demonstrate that the 266 nm stand-off Raman system can be used at eye-safe power densities to detect compounds commonly found in improvised explosives, such as Ammonium Nitrate and Nitromethane, at distances of 20 m and 12.5 m respectively, using a 100 mm diameter beam.

Statement of Original Authorship

The work contained in this thesis has not been previously submitted to meet requirements for an award at this or any other higher education institution. To the best of my knowledge and belief, the thesis contains no material previously published or written by another person except where due reference is made.

Signature:

Date: 21/1/15

Contents

List of Figures

List of Tables

Introduction

1

Sadly, it has become a frequently proven fact that no community is immune to the loss of life and injury caused by explosive devices. Whether inadvertently detonated or intentionally used as weapons, the physical and psychological damage that explosives and devices that contain them create can be immense. Unfortunately, it is possible to construct such devices from relatively easy to obtain materials without much prior knowledge or skill. Therefore, in order to protect the community, it is becoming increasingly more important to develop non-contact means of detection of explosive devices. This chapter gives an overview of the increasing use of explosive devices and describes some of the current detection techniques, with the intention of identifying accurate methods for ranged detection of explosives and other hazardous materials.

1.1 Increasing Use of Explosive Devices

Since 2004, the number of annual terrorist attacks worldwide has continued to grow each year, as shown in Figure 1.1.[1,2]

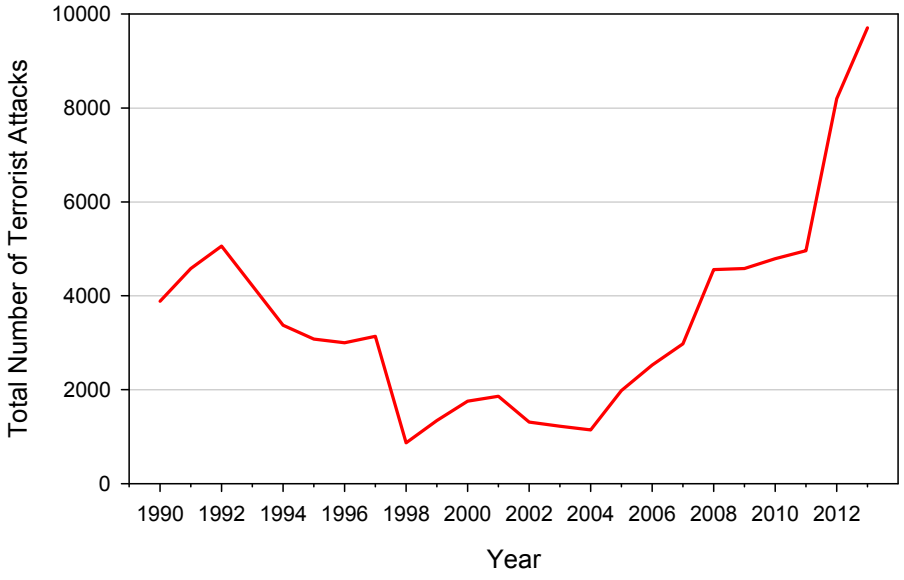

Figure 1.1: Number of terrorist attacks worldwide per year between 1990 and 2012.[1,2]

In 2012 the number of terrorist attacks worldwide was higher than in any other previous year with a 65% increase in attacks over that recorded in 2011.[1] The latest data shows that this trend continued in 2013, with the number of worldwide terrorist attacks increasing by a further 18% increase over those reported in 2012.[2] Alarmingly, not only is the number of attacks significantly increasing but so is the number of fatalities and injuries resulting from those attacks (Figure 1.2).

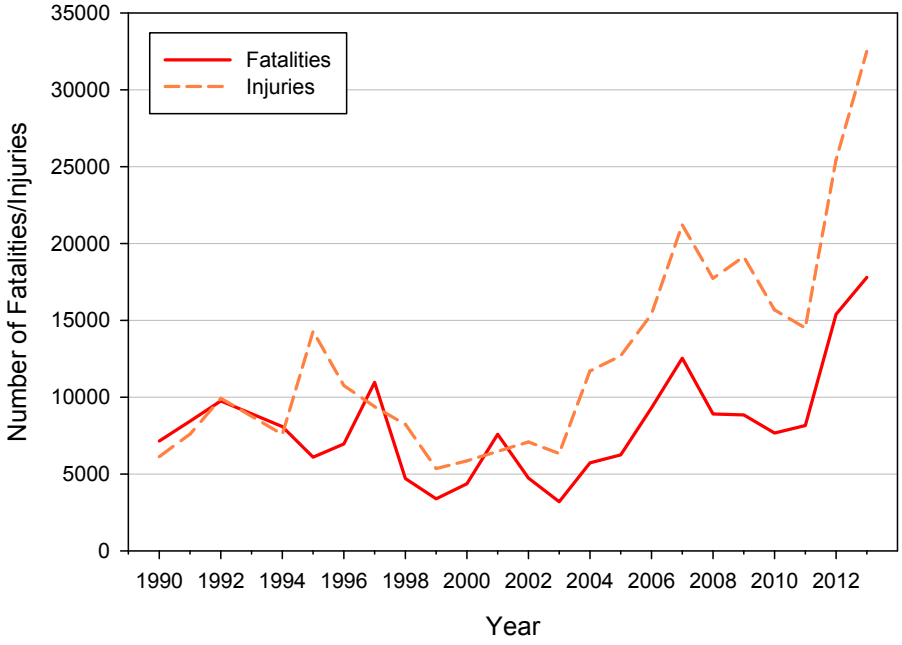

Figure 1.2: Annual injuries and fatalities worldwide due to terrorist attacks.[1]

Until 2013, 2012 contained the highest single year total of fatalities and injuries reported, with a total of 15,401 fatalities and 25,436 injuries resulting from terrorist attacks which is an 89% rise in fatalities and 76% more injuries than the amount that occurred in 2011. Recent data for 2013 shows that the number of annual fatalities and injuries continues to rise with a worldwide total of over 17,800 fatalities and 32,500 injuries in 2013.[2]

Analysis of the terrorist attacks carried out over the last 40 years reveals that there are several different weapon types used which includes:

- Explosives/Bombs/Dynamite
- Firearms
- Incendiary Devices
- Melee
- Chemical

The preferred weapon type used in terrorist attacks worldwide has varied over the past 40 years, in recent years there has been a growing number of attacks using firearms and explosives over other weapon types as shown in Figure 1.3. In 1994, the Explo-

sives/Bombs/Dynamite (EBD) category accounted for 34% of all the worldwide terrorist attacks for the year. However, since 1995 the number of attacks involving EBDs has risen substantially, with terrorist attacks involving EBDs in 2012 responsible for 64% of all terrorist attacks carried out in 2012. The number of worldwide attacks involving EBDs in 2012 was higher than in any other year and was almost double the number in 2011.

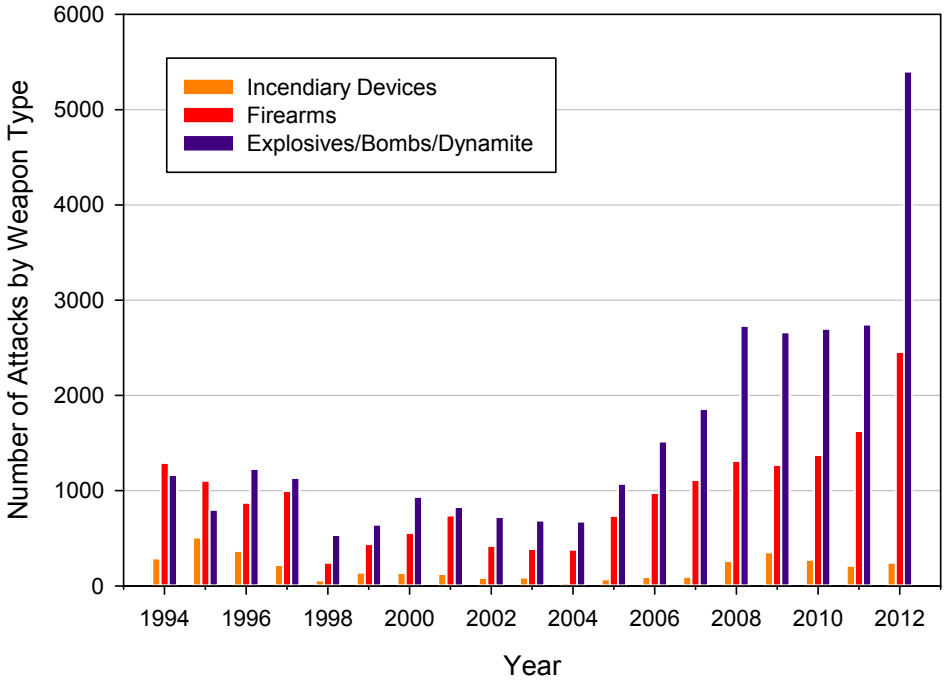

Figure 1.3: Number of worldwide terrorist attacks involving a particular weapon type between 1994 and 2012.[1]

In recent years, EBDs have caused the majority of fatalities and injuries in attacks worldwide, causing twice as many deaths than firearms between 2004 and 2012, as well as almost 8.5 times more injuries in the same peroid. Between 2003 and 2010, 11% of all civilian deaths (12,284 of 108,624) in Iraq were caused by suicide bomb events, averaging approximately 1,600 deaths per year from suicide bomb events alone.[3] In the United States of America there were 36,110 bombing incidents between 1983 and 2002, resulting in 5,931 injuries and 699 deaths and since 2002, that number continues to rise through attacks such as the Boston bombing in 2013.[4]

Figure 1.4 shows the spread of attacks involving EBDs, firearms and incendiary devices. Between 1994 and 2003, EBDs accounted for approximately 49% of the three, followed by firearms at approximately 40% and incendiary devices at approximately 11%. Between 2004 and 2012 the use of EBDs increased to approximately 62% of the three, with the usage of firearms down to approximately 33% and incendiary devices down to approximately 5%.

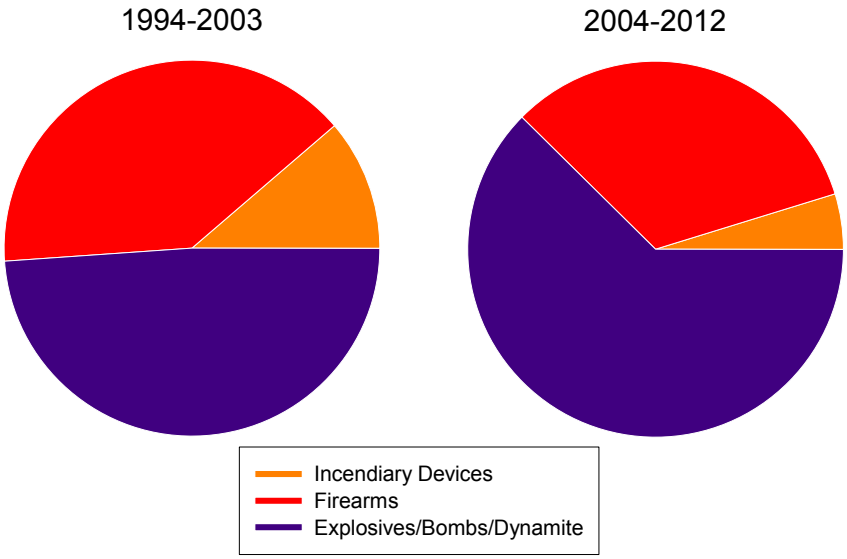

Figure 1.4: Difference in preferred terrorist weapon type between the 1994-2003 (left image) and 2004-2012 (right image) peroids.[1]

With an increase in the use of EBDs there is a growing need for an increase in security worldwide to detect these devices that are often concealed. Therefore, to safeguard the safety of the global population, it is essential that rapid, non-invasive and accurate methods for explosive detection in public places are developed.

1.2 Current Methods of Explosives Detection

There are many techniques used today for the detection and analysis of dangers such as chemicals weapons and explosives.[5,6] This section will briefly cover a few of the most common techniques used today, comparing their advantages and disadvantages.

1.2.1 Ion Mobility Spectroscopy

Ion mobility spectroscopy (IMS) was developed in the 1950's and 1960's, mainly by Earl W. McDaniel from the Georgia Institude of Technology, and exists in many different forms today.[7,8] The underlying method for all IMS techniques involves ionising the molecules of a sample, and then sending the resulting ions through a tube containing an applied electric field. The time of flight for the resulting ions through the tube can then be used to distinguish what the original molecular composition of the sample was. This is possible as different ions have a range of characteristics such as differing mass, charge, shape and size, causing variations in the time it takes for different ions to traverse the tube. This variance in time can be used to find the molecular structure of the original sample. IMS was originally used purely for detection of vapours, but it has since been adapted for use on liquid samples.[9] IMS is highly sensitive, relatively compact and can be set up as a

device for anyone to use, without needing knowledge of its inner workings. Currently IMS is used commercially as a common method for chemical hazards and explosive detection, particularly in airports and other areas of high security.

With all its advantages, there are a few major disadvantages to IMS which limit its applications for detection at distance. The biggest disadvantage to IMS is that a sample must be harvested and brought to an IMS device for testing, which could lead to loss of life and/or expensive equipment if the sample is hazardous. While the actual process of detection with IMS is quite rapid (of the order of milliseconds), collection of samples can be fairly time consuming. In situations where it is necessary to screen large numbers of individuals, the time intensive nature of the technique could make it impractical. For example, in screening people entering an airport, each person must be pulled aside for testing, which can take up to several minutes per person (depending on how thorough sample collection is). IMS is also quite invasive, requiring direct contact with a person and their belongings to collect a sample for testing.

1.2.2 Chromatography

Discovered in the early 1900's by Mikhail S. Tsvet, chromatography is a technique used for separating out different components of a solution.[10,11] By having a mobile phase (a liquid or gas containing the sample) flow through a stationary phase (a solid), different molecules in the sample will move at different rates, which can then be separated and extracted for analysis. Today there exists multiple methods for chromatography, all following the same underlying premise of its initial design.[12] Gas chromatography is usually used in conjunction with other methods such as IMS, described in Section 1.2.1.[13]

Unlike IMS, chromatography can require substantial time to separate differing molecules in a solution, with the fastest methods for chemical detection such as high-performance liquid chromatography (HPLC) still taking from several seconds up to several minutes for accurate results.[14,15] A sample must also be prepared for chromatography, requiring even more time before results are obtained and requiring operators to be in close proximity to the sample. As with IMS, approaching a sample for preparation and detection can be quite risky, and potentially lead to loss of life and/or expensive equipment. These disadvantages unfortunately make it impractical to use chromatography for real time explosive detection.

1.2.3 Infrared Spectroscopy

Infrared (IR) spectroscopy involves the use of light from the infrared region of the electromagnetic spectrum to determine the chemical composition of a sample. The use of

infrared light as a chemical detection tool was recognized in 1859 by Gustav Kirchhoff and Robert Bunsen, who realised that different substances had unique absorption and emmision spectra.[16] This eventually led to the first spectra of molecular vibrations in 1881 by Abney and Festing.[17,18] IR spectroscopy uses infrared light, which is absorbed by molecules causing them to vibrate or rotate. Since each vibration/rotation corresponds to a discrete energy state that is uniquely determined by the properties of the molecule, it is possible to identify the molecule by spectrally analysing the transmission of infrared light through the sample. As each unique molecule has unique vibrational modes, the extinction of light can be compared to a reference and the chemical composition can be determined.[19]

IR Spectroscopy is fast and efficient, with detection possible in under a second, and able to produce spectra from samples weighing a matter of grams.[20] The technique does not rely on a specific material phase, and is able to determine chemicals in gas, liquid and solid forms, with measurement possible without destruction of the sample. IR spectroscopy can also be used to determine information such as basic structural details and potential quantitative information. While IR spectroscopy has many benefits, it unfortunately has several issues which severely limit its ability to reliably detect hazards in the field. Spectra arrising from IR spectroscopy are often extremely complicated, with no clear way to identify the sample without using other methods, such as IMS spectroscopy. Some absorption bands for organic compounds are very close together, causing peaks to overlap and important information to become hidden under the overlapping peaks. Not every molecule provides a strong absorption peak, and some interactions inside certain molecules can cause spectra to become difficult to decipher.[21]

1.2.4 Terahertz Spectroscopy

Similar to IR spectroscopy, Terahertz (THz) spectroscopy involves probing the vibrational activity of a sample. THz spectroscopy uses light with frequencies in between 0.1 and 10 THz, that utilise vibrational modes outside the range of IR spectroscopy.[6,22] Some molecular rotations are also detectable in the THz region, giving more available information over IR spectroscopy. Like IR Spectroscopy, THz spectroscopy is fast and allows for scanning of samples in the order of seconds. One significant advantage of THz spectroscopy lies in its ability to penetrate packaging, such as those commonly made from plastics and fluorocarbons including Polyethylene (PTE) and Polytetrafluoroethylene (PTFE). While there appears to be promise in the use for explosive detection, this area of spectroscopy is still in its infancy and as a result its effectiveness is still yet to be fully explored.[23]

1.2.5 Raman Spectroscopy

Raman spectroscopy relies upon the use of Raman scattering, an inelastic subtype of light scattering first discovered by Sir Chandrasekhara Raman in 1928.[24] When a photon is incident upon a molecule, it is predominantly scattered through the more familiar elastic scattering process, known as Rayleigh scattering, in which the energy of the scattered photon is the same as that of the incident photon.[25] If a photon is incident upon a molecule as it is undergoing a change in energy, such as relaxing from a higher vibrational mode to a lower vibration mode or vice versa, the scattered photon can gain or lose this energy. This exchange in energy results in a change to the photons wavelength which can then be spectroscopically measured to reveal the molecular fingerprint of the material causing the scatter. Raman scattered light which has a lower energy than the incident light is known as the "Stokes" Raman component, and Raman scattered light which has higher energy than the incident light is the "anti-Stokes" Raman component as shown in Figure 1.5.[25]

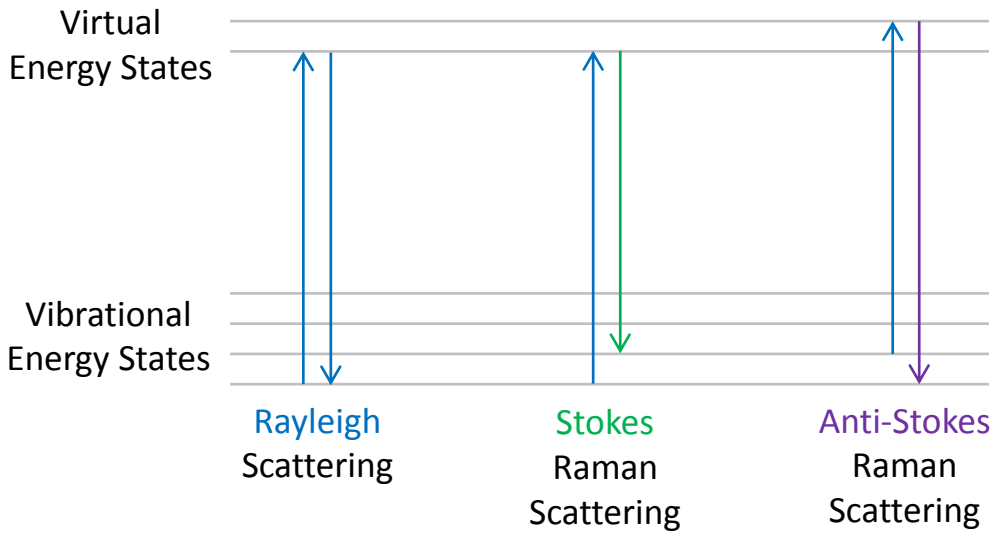

Figure 1.5: Energy change for different scattering processes.

As all samples at room temperature contain molecules mostly in the lowest possible energy state, Stokes Raman scattering provides larger Raman intensities for standard samples at room temperatures as shown in Figure 1.6.[26] Because every unique molecule presents unique energy states for certain excitations, whether it be vibrational, rotational, or via other excitations, Raman scattering can be used to determine the chemical composition of a sample. While this process appears to be familiar to IR spectroscopy and THz spectroscopy, Raman scattering is a purely scattering effect, with no delay from processes such as absorption and emmision. This means that the entire transition between incident photon and scattered photon occurs in a matter of femtoseconds, appearing almost in-

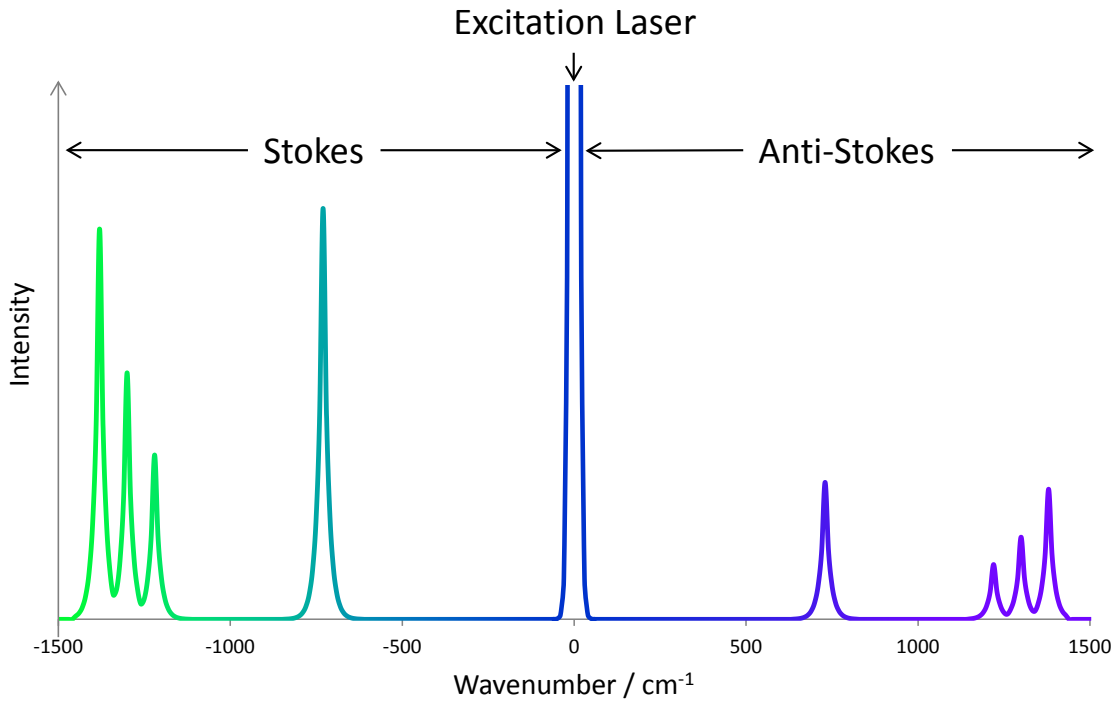

Figure 1.6: Intensity of Stokes and anti-Stokes Raman bands.

stantaneously. The ratio of photons which undergo Raman scattering from a sample is rather low, with only approximately 1 in every 10 million photons scattered by the Raman effect, which means a large number of incident photons are required to accurately detect a compound.[27] Advances in filters to remove and surpress unwanted light assists detection of the Raman signal, and with the advances in laser optical systems it is now possible to produce the high incident photon fluxes necessary to make Raman scattering a relatively cheap and very effective method for chemical fingerprinting.[27]

1.3 Considerations for Detecting Explosives at Distance

There are several important attributes to consider when determining which method is most suitable for the detection of chemical hazards and explosives at distance. The most important of these include:

- Detection speed
- Safety of personel and civillians
- Invasiveness of method
- Strength of detected signal
- Potential damage to detection equipment

As described in the previous sections, Raman spectroscopy is a promising detection method which has significant advantages over alternatives for fast non-contact detection of mate-

rials.[28–32] Since Raman scattering is a fast optical process, detection timescales are short and since laser beams have low beam divergences, it is possible to make a non-invasive measurement at distances of the order of several hundreds of metres from a suspicious sample.[33,34] Because of this potential, the application of Raman spectroscopy for ranged detection of compounds is of much interest to security agencies, commercial entities and researchers, and has become known as "stand-off Raman spectroscopy". Fast detection being possible from such great distances is of great importance when dealing with explosive detection, where detection a few seconds earlier, or at distances further away, could make a difference in the number of lives saved.

While stand-off Raman spectroscopy can achieve accurate and rapid results when used for ranged chemical detection, the radiant exposures of the lasers used are often extremely high and are at levels that can cause significant eye or skin injury in the event of unexpected exposure. For this reason, the laser emission from a stand-off Raman system must be analysed to ensure it does not exceed recognized safe levels, so that detection of chemical hazards and explosives at range in public is achievable with minimal risk of injury to bystanders. Restricting the laser emission to safe levels will result in some sacrifice in the Raman signal intensity if the laser is to be operated in public. Clearly a necessary step in the design and implementation of a functional stand-off Raman system usable in the field will involve determining what combination laser parameters provide the best possible Raman intensities, while still ensuring that the laser emission remains safe and incapable of injuring the eye or the skin. In the following chapter, the impact that various laser parameters have on the Raman signal will be considered. In doing this, the parameter ranges used are reflective of the commercially available equipment that is typically used for stand-off Raman detection of this type.

Theoretical Description of the Intensity of Raman Scattering

2

In this chapter, the dependence of the Raman signal magnitude on laser and other system parameters is examined from both a theoretical and practical perspective, to allow accurate projections of detection limits to be made. Since the theory of Raman scattering of light from molecules has been well established since its discovery nearly 100 years ago, a detailed theoretical exposé of the effect is unnecessary here. Instead a brief overview focussing on the essential features with regard to the stand-off application discussed in this thesis will be provided as a background. In particular, the dependence of the Raman scattering intensity on, the excitation wavelength and its proximity to material resonances, the excitation pulse energy and, how the detected Raman signal varies with sample distance will be canvassed.

2.1 Wavelength Dependence

The Raman scattered light from a sample results from an oscillating electric dipole of the molecules,[35] which is induced by an incident electric field which can be expressed as a time-dependent vector of incident radiation $\boldsymbol{E}$, oscillating at a frequency ν. The total time-dependent induced electric dipole moment vector, $\boldsymbol{\mu}$, of a single molecule can be modelled as a Taylor series expansion of induced electric dipole moment orders that correspond to different powers of electric field amplitude:

$$\boldsymbol{\mu} = \boldsymbol{\mu}^{(1)} + \boldsymbol{\mu}^{(2)} + \boldsymbol{\mu}^{(3)} + \dots \ , \tag{2.1.1}$$

where

$$\boldsymbol{\mu}^{(1)} = \boldsymbol{\alpha} \cdot \boldsymbol{E}, \tag{2.1.2a}$$

$$\boldsymbol{\mu}^{(2)} = \frac{1}{2}\boldsymbol{\beta} : \boldsymbol{E}^2, \tag{2.1.2b}$$

$$\boldsymbol{\mu}^{(3)} = \frac{1}{6}\boldsymbol{\gamma} \vdots \boldsymbol{E}^3, \tag{2.1.2c}$$

with $\boldsymbol{\alpha}$, $\boldsymbol{\beta}$ and $\boldsymbol{\gamma}$ representing the polarisability, hyperpolarisability and second hyperpolarisability tensors respectively. Equation (2.1.2a) gives the most dominant term in the expansion, $\boldsymbol{\mu}^{(1)}$, which is proportional to the incident field strength, while the first two nonlinear terms are given by Equation (2.1.2b) and Equation (2.1.2c) which are the quadratic and cubic terms, $\boldsymbol{\mu}^{(2)}$ and $\boldsymbol{\mu}^{(3)}$ respectively. Nonlinear terms of Equation (2.1.1) are negligible at low intensities as is typically the case in most Raman spectroscopy setups and therefore, the linear term $\boldsymbol{\mu}^{(1)}$ is generally a very good approximation of the total induced dipole moment. Using this linear term shown in Equation (2.1.2a) as the total dipole moment vector equation and neglecting the nonlinear terms:

$$\boldsymbol{\mu} \approx \boldsymbol{\mu}^{(1)} = \boldsymbol{\alpha} \cdot \boldsymbol{E}. \tag{2.1.3}$$

The intensity I of scattered light, which is radiated by an oscillating electric dipole with amplitude μ_0 of a single molecule, which has been induced by an electric field E of frequency ν, can be expressed by the equation[35]

$$I = \frac{\nu_d^4 \mu_0^2 \sin^2\theta}{32\pi^2 \epsilon_0 c^3}, \tag{2.1.4}$$

where θ is the angle at which the incident light makes with the axis of the dipole, ν_d is the frequency of the induced electric dipole (which is usually but not always equal to ν), c is the speed of light, and ϵ_0 is the permittivity of free space. As the magnitude of the total time-dependent induced electric dipole moment vector shown in Equation (2.1.3), μ_0, depends on the frequency of the induced electric dipole, ν_d, it can be separated into the Rayleigh scattering and Raman scattering components:

$$\boldsymbol{\mu}_0(\nu) = \boldsymbol{\alpha}^{Ray} \cdot \boldsymbol{E}_0(\nu) \qquad \text{for Rayleigh scattering,} \tag{2.1.5a}$$

$$\boldsymbol{\mu}_0(\nu \pm \nu_m) = \boldsymbol{\alpha}^{Ram} \cdot \boldsymbol{E}_0(\nu) \qquad \text{for Raman scattering,} \tag{2.1.5b}$$

where $\boldsymbol{\mu}_0(\nu)$ and $\boldsymbol{\mu}_0(\nu \pm \nu_m)$ are the time-independent amplitudes of the induced electric dipole of frequency ν and $\nu \pm \nu_m$ respectively, ν is the frequency of the incident electric field, and ν_m is a virtual molecular frequency. $\boldsymbol{E}_0(\nu)$ is the time-independent amplitude of the incident electric field, $\boldsymbol{\alpha}^{Ray}$ is an equilibrium polarisability tensor and $\boldsymbol{\alpha}^{Ram}$ is a polarisability tensor corresponding to ν_m.

The square of Equation (2.1.5b) can be represented in component form through combination with the angular dependence in Equation (2.1.4), transforming the coordinate frame from the dipole of the molecule into the coordinate frame of the scattered and incident light:[36]

$$\mu_0^2(\nu \pm \nu_m)\sin^2\theta = \left|\boldsymbol{E}_0(\nu)\right|^2 \sum_{ij} \left|\boldsymbol{\alpha}_{ij}^{Ram}\right|^2, \tag{2.1.6}$$

where i is the direction of the scattered light, j is the direction of the incident light, and $\boldsymbol{\alpha}_{ij}^{Ram}$ is the (i, j)th component of the Raman polarisability tensor in Equation (2.1.5b). So for the case of purely Raman scattered light, substituting equation (2.1.6) into (2.1.4) gives an expression for the intensity of Raman scattered light:

$$I_{Raman} = \frac{(\nu \pm \nu_m)^4 \left|\boldsymbol{E}_0(\nu)\right|^2}{32\pi^2\epsilon_0 c_0^3} \sum_{ij} \left|\boldsymbol{\alpha}_{ij}^{Ram}\right|^2. \tag{2.1.7}$$

Equation (2.1.7) and Equation (2.1.4) are only strictly valid for light scattered from objects much smaller than the wavelength of the incident light. At first this may appear unrealistic as often the materials under interrogation are macroscopic solids. However, the Raman scattering occurs from the chemical bonds between molecules, which are of the order of angstroms,[37] and are thus 3 orders of magnitude smaller than the wavelength of any available laser. Equation (2.1.7) shows that the Raman signal intensity depends on the fourth power of the frequency (ν^4), or in terms of wavelength (λ), a λ^{-4} dependence. Therefore incident light at shorter wavelengths will provide much larger intensities of Raman scattered light compared to those obtained at longer wavelengths.

2.2 Energy Dependence

In addition to the frequency dependence, Equation (2.1.7) from Section 2.1 also shows that the intensity of Raman scattered light from a single molecule is proportional to the square of the amplitude of the electric field component of the incident light:

$$I_{Raman}(\text{Single Molecule}) \propto \left|\boldsymbol{E}_0(\nu)\right|^2. \tag{2.2.1}$$

The total energy, $\hat{H}$, stored in the electric field of an electromagnetic field is given by[38]

$$\hat{H} = \frac{1}{2}\epsilon \int_V \left|\boldsymbol{E}_0(\nu)\right|^2 \mathrm{d}V, \tag{2.2.2}$$

where ϵ is the permittivity of the medium in which the electric field is travelling through, and V is a given volume. From Equation (2.2.1) and Equation (2.2.2) it is apparent that the intensity of the total Raman scattered light depends linearly on the total energy of the incident light:

$$I_{Raman} \propto \left|\boldsymbol{E}_0(\nu)\right|^2 \propto \hat{H}. \tag{2.2.3}$$

2.3 Material Dependence

The molecular make-up of the sample material will influence the Raman signal intensity detected. In the context of the stand-off Raman application discussed in this thesis, the

two material attributes of most significance are the proximity of any energy resonances to the incident photon energy, and the level of fluorescence produced by the sample. Both of these will be discussed in this section.

2.3.1 Resonance and Pre-resonance Dependence

Resonance Raman (RR) scattering occurs when the frequency of light incident upon a molecule is resonant with an electronic transition of that molecule, causing an enhancement in the intensity of Raman scattered light. If the incident light is not actually resonant, but is close to being so, then some signal enhancement still occurs and is said to result from pre-resonance Raman (PRR) effects.[35,39] Enhancement through these resonant effects can be up to 6 orders of magnitude greater than when nonresonant, depending on the proximity of the frequency of the incident laser to the electronic transition of the molecule being examined.[40] As many explosives are organic in nature, and contain electronic transitions in the ultraviolet (UV) and deep ultraviolet (DUV) regions of the electromagnetic spectrum, RR and PRR using UV lasers have proven to be particularly effective at detecting trace amounts of explosives, even at stand-off distances of several metres.[40,41]

While the rigorous theory behind RR and PRR is quite complex,[35] for some materials approximations can be used that greatly simplify the expressions describing the enhancement of Raman signal intensity when near resonance, such as the work by Dudik *et al.*,[42] and Asher:[43]

$$\sigma_{PRR} = \sqrt{K}\Big[\frac{\nu_e^2 + \nu^2}{(\nu_e^2 - \nu^2)^2}\Big], \tag{2.3.1}$$

where K is a constant specific to the Raman transition, ν_e is the frequency of a resonant electronic transition, and ν is the frequency of the incident laser. As Equation (2.3.1) is an element of the polarisability tensor, $\sum_{ij} \boldsymbol{\alpha}_{ij}^{Ram}$, from Equation (2.1.7) shown in Section 2.1, the intensity of Raman scattered light due to PRR will scale quadratically with σ_{PRR} from Equation (2.3.1) by

$$I_{Raman} \propto \sum_{ij} \left|\boldsymbol{\alpha}_{ij}^{Ram}\right|^2 \propto \sigma_{PRR}^2 = K\Big[\frac{\nu_e^2 + \nu^2}{(\nu_e^2 - \nu^2)^2}\Big]^2. \tag{2.3.2}$$

2.3.2 Fluorescence Dependence

One significant difficulty of applying Raman spectroscopy for material detection is the extremely low signal to noise ratios that result, due to the inherently low Raman photon count compared to the photon fluxes produced by other scattering and emission processes (as described in Section 1.2.5). In particular, if a sample or contaminant within strongly fluoresces, a Raman signal can be swamped by this undesirable noise at the detector.

Fluorescence is highly material dependent, and while this can be problematic, it can be reduced through choice of excitation wavelength since the level fluorescence produced is also dependent on wavelength. Typically, fluorescence occurs in the wavelength region between 260 nm and 900 nm for most materials. Raman spectroscopy using DUV excitation has shown negligible fluorescence to the point where wavelengths below 265 nm are known as the "fluorescence free Raman region".[44] Avoiding incident light of wavelengths in regions of high fluorescence will allow Raman signals to be easily more detected, resulting in much higher signal to noise ratios.

2.4 Distance Dependence

While the direction of light scattered by a single scatterer depends on both the direction of the incident light and the orientation of the dipole,[35] a sample which is not perfectly crystalline will on average contain a random distribution of a large number of scatterers. The cumulative effect is to scatter the incident light isotropically. Therefore, like an isotropically point source emitter, the intensity of the Raman scattered light from a noncrystalline sample will fall away as the inverse square of the distance of the sample from the detector by

$$I \propto \frac{1}{d^2}, \tag{2.4.1}$$

where d is the collection distance, being the distance between the sample and the collection optics.

Raman scattering is accurately described by this inverse square law, as long as the diameter of the collection lens is of sufficient size when compared to the diameter of the beam on the sample being irradiated. Due to the collection optics having a finite field of view, the efficiency for scattered collection will decrease if the beam size becomes too large for the field of view for the collection lens. Assuming that the relative size of the collection optics and the excitation beam diameter are suitable, the relationship between Raman intensity and collection distance can be expressed as

$$I_{Raman} \propto \frac{1}{d^2}. \tag{2.4.2}$$

2.5 Combined Impact on Raman Signal Intensity

Combining the factors that determine the Raman signal intensity covered in this chapter, allows comparisons between Raman scattering intensities obtained under different laser and sample conditions. Equation (2.1.7) and Equation (2.2.3) capture the dependence of

Raman intensity on the wavelength and energy of the incident light used, while Equation (2.4.2) shows the change in Raman intensity with varying collection distance. Finally, Equation (2.3.2) displays the change in Raman intensity resulting from pre-resonance Raman based on incident wavelength and the material used. Combining all of these effects allows Raman signal comparisons to be theoretically made for differing laser and material parameters using

$$I_{Raman} \propto \frac{\hat{H}(\nu \pm \nu_m)^4}{d^2}\left[\frac{\nu_e^2 + \nu^2}{(\nu_e^2 - \nu^2)^2}\right]^2, \tag{2.5.1}$$

where this approximation is only strictly valid under low incident intensities of light, as discussed during Section 2.1. As evident from the dependencies given in Equation (2.5.1), the frequency of the incident light used has a strong impact on the intensity of Raman scattered light, along with an inverse square relationship on the collection distance from the sample, and a linear dependence on the energy of the incident light used. For example, doubling the excitation wavelength will result in a 16 fold decrease in Raman signal, as will quadrupling the detector to sample distance.

The analysis so far will allow determining conditions under which the Raman signal can be maximized through choice of wavelength and other beam parameters. However, these same parameters dictate the maximum emission that the laser can radiate without risk of injury to the eye or skin. It is possible, and indeed likely, that the beam properties that optimize the Raman signal intensity may result in laser emissions that are more hazardous than that produced by an alternate laser configuration that produces a lower Raman signal intensity. Determining the laser parameters that allow a maximum possible Raman signal to be safely obtained with an exposed and accessible laser beam in public areas, is an imperative for stand-off Raman operations in the field. This will allow for the rapid and non-invasive scanning of potential hazards in public locations, at a safe operation distance. The following chapter will investigate the safe exposure levels for laser systems that are typically used for Raman spectroscopy, with the intention to determine conditions that yield the maximum possible Raman signal that result with safe levels of laser radiation.

Evaluation of Safe Levels of Laser Emission

3

It is well documented that over exposure to radiation can have damaging effects on biological matter, and that it is a complicated combination of factors such as the properties of the radiation, the amount of incident radiation, and the type of biological matter on which the radiation is incident upon, that determine the nature and severity of any damage. To protect individuals from over exposure to coherent non-ionizing radiation produced by lasers, most nations employ standards that describe what is deemed to be a safe level of exposure to any given laser source. Using these standards to determine safe radiation levels can be complex, and depend on a number of factors including:

- The wavelength of the laser light
- The pulse duration for a pulsed laser system
- The pulse repetition frequency for a pulsed laser system
- The section of the body exposed (skin or eye)
- The length of time that exposure occurs
- The angular subtense of the laser beam

All of these variables must be considered to determine what constitutes a safe level of emission from any laser system, to ensure it is deployable in the field for stand-off Raman detection.

The safe level of emission for any pulsed laser system are expressed in terms of a radiant exposure, being an amount energy incident upon a given area. The standards that proscribe the safe exposure levels refer to these radiant exposures as the 'Maximum Permissible Exposure' (MPE) and usually they are expressed in the units of Joules per metres squared (J/m^2). When high levels of radiation are potentially absorbed by biological tissue, heating can occur which ultimately leads to thermal damage of the tissue. With knowledge of the threshold at which this thermal damage occurs in certain tissues such as the eye or skin, limitations on maximum emissions of radiation can be derived, allowing for the calculation of the MPE. In the following sections the MPEs for a range of different wavelengths and other laser parameters will be evaluated, with the aim of identifying the

parameter set that yields the highest MPE and therefore identifying the wavelengths at which the highest pulse energies can be used safely.

3.1 Maximum Permissible Exposures for Pulsed Laser Systems

The MPE for any laser system can be calculated using guidelines provided by various international and/or national standards. Two laser safety standards that are routinely used throughout North America and large parts of Europe for MPE calculation are the American National Standard for Safe Use of Lasers (ANSI Z136.1) and the International Electrotechnical Commission (IEC 60825-1).[45,46] Australia has adopted the European standard which is published as the Australian standard AS/NZS IEC60825.14:2011.[47] The discussion of MPEs in this chapter will exclusively use the calculation methodology of AS/NZS IEC 60825.14:2011,[47] which are adopted from the 2007 revision of IEC 60825-1, found in IEC/TR 60825-14.[46] However, it should be noted that the American standard and the European standard are consistent in that the MPE evaluated following the procedures outlined in them are the same. Following the guidelines in the Australian standard, the MPE to exposure to pulsed laser emission was determined. For pulsed lasers there are at most three conditions that apply, with condition c) only applicable to ocular exposure from lasers with an excitation wavelength higher than 400 nm and only applicable to individual pulse durations shorter than 0.25 seconds long:[47]

a) The exposure from any single pulse within a pulse train shall not exceed the MPE for a single pulse.

b) The average exposure for a pulse train of exposure duration T shall not exceed the MPE for a single pulse of exposure duration T.

c) The average exposure from pulses within a pulse train shall not exceed the MPE for a single pulse multiplied by $N^{-1/4}$.

Where N is the number of pulses expected in an exposure.

The most restrictive (ie the lowest radiant exposure) of the three evaluated MPE is then used as the MPE available for comparison with the emission from a given laser system. Since the absorption properties of the eye and skin are significantly different, the MPEs for the skin and eye can be, and often are, very different. In this work we restrict some of the laser parameters to values that are limited by commercial availability of laser sources. For example, common pulsed laser system used for many applications are Q switched solid state lasers that have pulse durations of the order of 5 ns, and a pulse repetition frequency

of 10 Hz, an angular subtense of 1.5 mrad (ie the emission has a single mode Gaussian spatial distribution). In addition as we want to achieve rapid detection we assume an exposure time of 1 second. The MPE for both the eye and skin to this type of emission was evaluated over a range of wavelengths, with the calculations for the MPEs of some common excitation wavelengths displayed in Appendix A.1, and their MPEs shown in Table 3.1. The MPEs over a range of wavelengths are shown in Figures 3.1 and 3.2.

Table 3.1: MPEs for some common excitation wavelengths for an exciation laser with a 5 ns pulse duration, a pulse repetition of 10 Hz, an angular subtense of 1.5 mrad, and an exposure time of 1 second.

Excitation Wavelength (nm)	Ocular MPE (J/m^2)	Skin MPE (J/m^2)	Available MPE (J/m^2)
266	3	3	3
355	47	47	47
532	0.0028	200	0.0028
785	0.004	296	0.004
1064	0.03	1000	0.03

From Figures 3.1 and 3.2, it is clear that for emission with these characteristics, the MPE for the skin and eyes differs in the visible (Vis) and near infrared (NIR) regions.

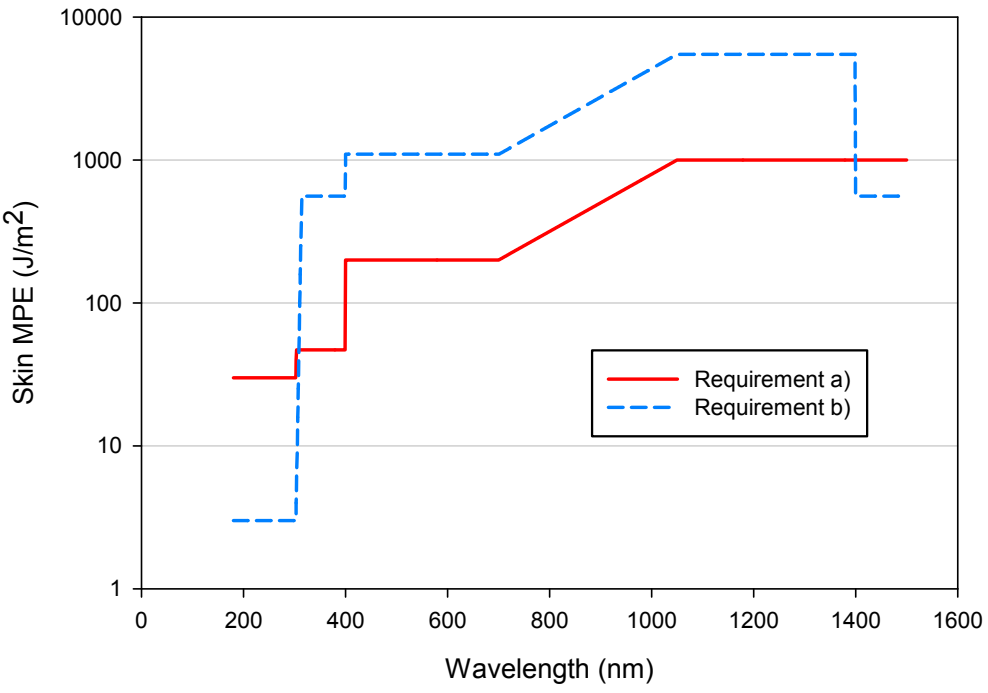

Figure 3.1: MPE for skin over a range of wavelengths with a 10 Hz pulsed laser having 5 ns pulse duration, 1 mrad angular subtense and a 1 second exposure time.

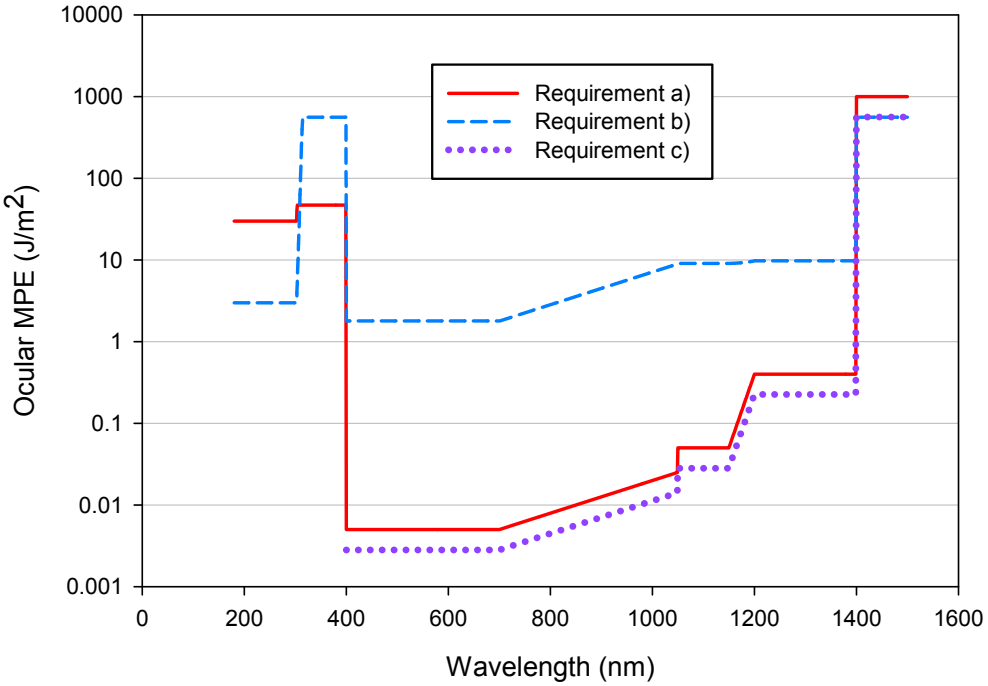

Figure 3.2: MPE for eyes over a range of wavelengths with a 10 Hz pulsed laser having 5 ns pulse duration, 1 mrad angular subtense and a 1 second exposure time.

Since the ocular MPE is more restrictive than the skin MPE for this combination of laser parameters, it will be used as the overall MPE and is shown in Figure 3.3.

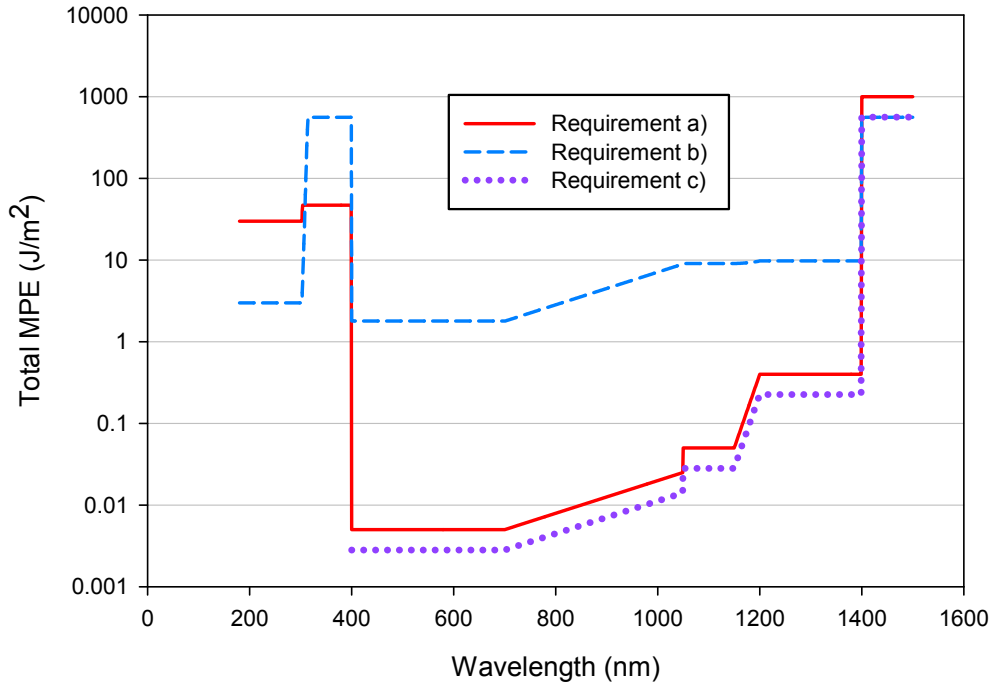

Figure 3.3: Total MPE over a range of wavelengths with a 10 Hz pulsed laser having 5 ns pulse duration, 1 mrad angular subtense and a 1 second exposure time.

Figure 3.4 shows the MPE, defined as the most restrictive of the three MPE values from requirements **a)**, **b)** and **c)** shown in Figure 3.3, for a range of wavelengths.

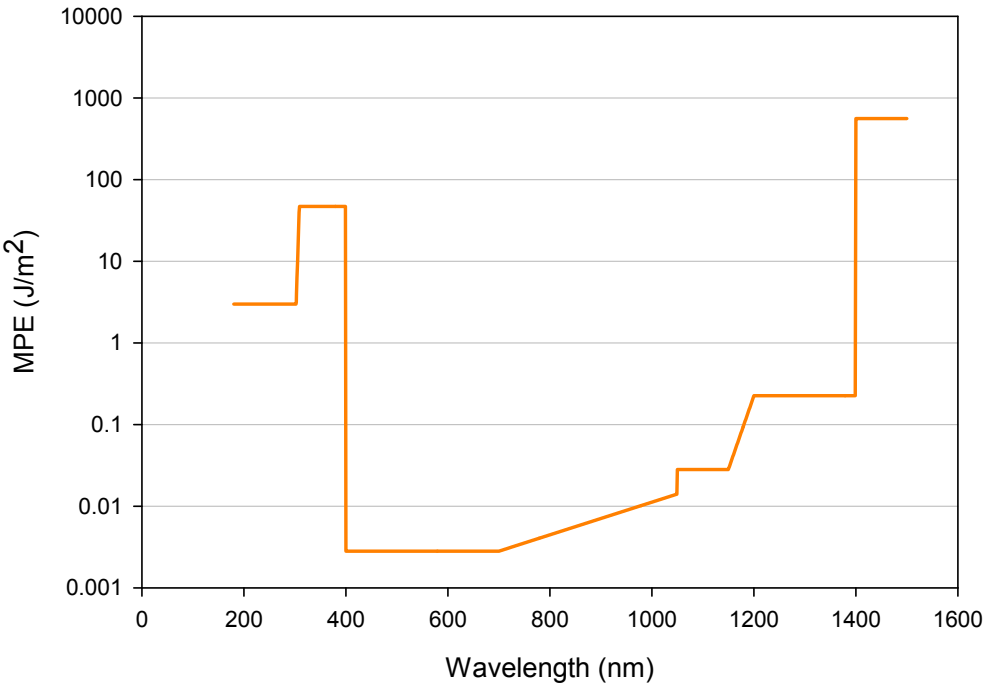

Figure 3.4: Best possible MPE over a range of wavelengths with a 10 Hz pulsed laser having 5 ns pulse duration, 1 mrad angular subtense and a 1 second exposure time.

Figure 3.4 shows that for Q switched nanosecond pulsed lasers, the highest MPE is found in the IR region of the spectrum at wavelengths greater than 1400 nm, while the lowest MPE is in the visible section of the spectrum. This is not surprising given the eyes sensitivity to visible light. Overall, it is then possible to use much higher radiant exposures in the IR and UV parts of the spectrum, without the same risk of injury than an equivalent radiant exposure in the visible. The radiant exposures at each wavelength can be converted into an equivalent single pulse energy by multiplying the MPE by the appropriate limiting aperture area for that wavelength which are listed in Appendix A.2.

As discussed in Sections 2.1 and 2.2, and given by Equation (2.1.7), the intensity of Raman scattered light depends on both excitation pulse energy and wavelength. Therefore, by using the energy and wavelength dependence given in Equation (2.1.7), and the MPE equivalent pulse energy, the relative Raman signal intensity at each wavelength can be determined when resonance effects are ignored. The results of this evaluation are shown in Figure 3.5 and this graph shows the resulting relative Raman signal strengths assuming a pulse energy equivalent to the MPE and ignoring resonance effects. In addition here it has been assumed that the collection efficiency of the detector is the same at all wavelengths.

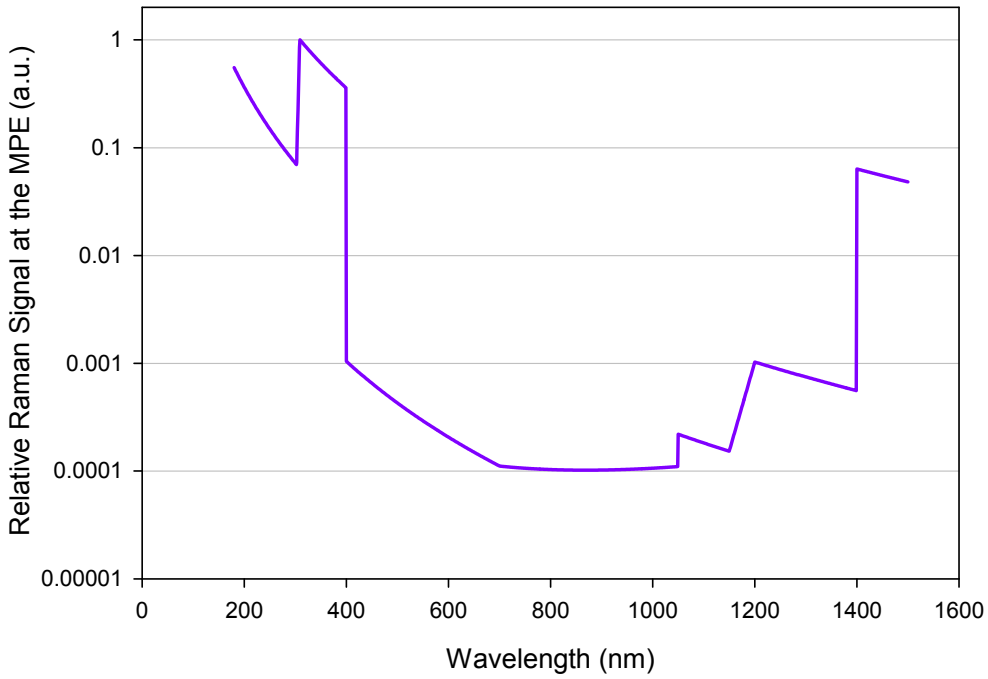

Figure 3.5: Relative Raman signal at the MPE over wavelength.

Figure 3.5 shows that the highest Raman signal intensities can be obtained at safe emission levels in the UV region of the spectrum. In the UVA region, Raman signals are up to an order of magnitude higher than signals in the UVB, UVC and the IR region between 1.4 and 1.5 microns. Raman signals in the UVA produced by a laser pulse energies corresponding to the MPE, are between 1000 and 10,000 times more intense than those generated by 'safe' lasers in the visible and NIR regions. In addition, further Raman signal enhancement in the UV region is possible through pre-resonance, which is sample dependent as discussed in Section 2.3.1. Fortunately, as many explosives have electronic transitions in the UV region it is highly likely that further Raman signal intensity increases will be possible when 'safe' UV lasers are used in stand-off mode to detect explosives, over the signals possible with 'safe' Vis/NIR or IR excitation lasers.[40]

3.2 Is Stand-off Raman Detection Possible at MPE Equivalent Pulse Energies?

Many studies exist which show the effectiveness of Raman spectroscopy for detecting materials over impressive stand-off distances with different laser parameters. However, in all of these studies, optimising the Raman signal and as a result the detection range is the over riding aim and issues such as eye and skin safety are often a minor consideration. While this is acceptable in well controlled environments where control measures such as personal protective equipment (PPE) are readily implemented, it is not in the field

where it is difficult or impossible to implement such safety precautions. For stand-off Raman spectroscopy to be used in a field application where control measures are hard to implement, it is imperative that the radiant exposures of lasers used must be at or below the MPE, but still generate a Raman signal that is greater than the background noise.

By using the dependence of the detected stand-off Raman signal intensity on wavelength, pulse energy, detector distance and resonance effects, as given by Equation (2.5.1), it is possible to determine the maximum detection range at each wavelength while keeping the laser emission below the MPE. Here it is again assumed that the detector collection efficiency is the same at each wavelength and that the detector noise is the same at each wavelength. Using this relationship, we can calculate the ratio of maximum detection range between two different wavelengths. In each case the maximum detection range is defined to be the distance at which the Raman signal intensity falls to 1 detector count. Without considering material dependent factors such as pre-resonance gains or fluorescence losses, the ratio of maximum detection range between two 'safe' laser systems is

$$\frac{d_{\lambda_1}}{d_{\lambda_2}} = \left(\frac{\lambda_2}{\lambda_1}\right)^2 \sqrt{\frac{M_{\lambda_1}}{M_{\lambda_2}}}, \tag{3.2.1}$$

where d_{λ_1} is the maximum detection distance of a laser at wavelength λ_1, d_{λ_2} is the maximum detection distance of a laser at wavelength λ_2, M_{λ_1} is the MPE at wavelength λ_1, and M_{λ_2} is the MPE at wavelength λ_2.

Equation (3.2.1) gives an example, where two commercial lasers at wavelengths of 266 nm and 532 nm, which have respective MPEs of 3 J/m^2 and 2.8 mJ/m^2 (Table 3.1 and Figure 3.3):

$$\frac{d_{\lambda_{266}}}{d_{\lambda_{532}}} = \left(\frac{\lambda_{532}}{\lambda_{266}}\right)^2 \sqrt{\frac{M_{\lambda_{266}}}{M_{\lambda_{532}}}} \approx 131. \tag{3.2.2}$$

At 266 nm the maximum safe pulse energy is many orders of magnitude greater than at 532 nm. In addition the Raman scattering efficiency at 266 nm is significantly larger than at 532 nm. Combining these, results in a detection range that is approximately 131 times larger at the shorter wavelength as shown by Equation (3.2.2). Further increase in maximum detection distance is potentially available at 266 nm through the material dependent factors discussed in Section 2.3, such as pre-resonance effects.

While theoretically, the dependence of the Raman signal intensity on parameters such as wavelength, energy and detector distance as discussed in Chapter 2, is well accepted, it is important to validate that they hold for a practical stand-off Raman system. This is essential if Equation (2.5.1) is to be used to compare maximum Raman ranges at different wavelengths. Chapter 4 describes the results of a range of experiments performed to validate Equation (2.5.1) and by extension, Equation (3.2.2). In addition, in Chapter

4, stand-off Raman spectroscopy experiments are described where radiant exposures less than the MPE are used to confirm that it is possible to use safe emission levels and to use Raman spectroscopy to rapidly detect materials at distance.

Experimental Raman Signal Comparisons

4

Chapter 2 provided a brief overview of the well established theoretical dependence of the Raman signal, on experimental parameters such as excitation wavelength, incident pulse energy and the distance of the sample from the collection optics. Using these relationships, along with the MPEs found in Chapter 3, it was predicted that the maximum operating range of a 'safe' 266 nm stand-off Raman system would be 131 times larger than that of an equivalent 'safe' 532 nm system. However, while there is no doubt that the analysis outlined in Chapter 2 is theoretically sound, there are many practical experimental factors that may lead to the signals produced by an actual stand-off Raman system that do not display the expected theoretical behaviour. For example, if the photometric response of the detector is not linear, then the inverse square dependence of the Raman signal on sample distance will not hold.

The intention of this chapter is to verify that the theoretical dependence of signal on incident energy, excitation wavelength and sample distance as given in Chapter 2, are valid for practical stand-off Raman systems operating at 266 nm and 532 nm wavelengths. This experimental investigation involved monitoring the resulting change in Raman signal intensity from a sample when excitation parameters such as the incident pulse energy or radiant exposure were varied, or, by varying collection parameters like the sample distance, and accumulation time of the camera's CCD. While some of the equipment used for each comparison at the two wavelengths was common, such as the Raman spectrometer and CCD array, other components such as the laser head and collection optics were wavelength specific. Any variation due to the wavelength dependence of the components used was corrected for, an example being the known wavelength dependence of the CCD array's quantum efficiency being corrected for in the comparisons. Table 4.1 lists the key specifications of the equipment used for the experimental comparisons.

Table 4.1: Table of equipment used in experiments throughout this chapter, along with key specifications at both 266 nm and 532 nm wavelengths.

Item with Key Attributes	**266 nm Specifications (a)**	**532 nm Specifications (b)**
1. Quantel Brilliant EaZy Nd:YAG 1064 nm Laser	Frequency Quadruple Module	Frequency Doubling Module
Pulse Energy Range:	0.1 mJ to 50 mJ	0.1 mJ to 100 mJ
Pulse Duration Range:	5 ns to 20 ns	5 ns to 20 ns
Repetition Rate:	10 Hz	10 Hz
Beam Diameter:	1 mm	1 mm
2. Spectrometer	UV Holographic Diffraction Grating	Blaze Visible Diffraction Grating
Grating Spacing:	2400 gratings/mm	1200 gratings/mm
Grating Efficiency ($QE_{Grating}$):	42%	72%
3. Nd:YAG Laser Plano Metallic Coated Mirrors	4th Harmonic	2nd Harmonic
Diameter:	6 cm	6 cm
45° Reflection:	>99%	>99%
4. Bi-Convex Focusing Lenses	266 nm Antireflection Coating	532 nm Antireflection Coating
Diameter:	6 cm	6 cm
Focal Length:	5 cm	6 cm
5. Semrock RazorEdge Ultrasteep Long-pass Edge Filter	266 nm Filter	532 nm Filter
Filter Transmission (QE_{Filter}):	76%	99.9%
6. Beam Collimator	266 nm Optics	532 nm Optics
Collimated Diameter:	20 mm	20 mm
7. Princeton Instruments PI-MAX4 ICCD Camera		
CCD Quantum Efficiency (QE_{CCD}):	6%	15.5%
8. Princeton Instruments LG-455-020 Fibre Optic Cable		
Wavelength range: 190 to 1100 nm		
9. Polytetrafluoroethylene (Teflon)		
10. Translational Stage		
11. Adjustable Apertures		
12. Lightfield Software		
13. Ammonium Nitrate		
14. Hydrogen Peroxide		
15. Nitromethane		
15. Laser Power Meter	Reading accuracy ±1%	Reading accuracy ±1%

In the following sections, experiments will be described that use the components listed in Table 4.1 to compare the Raman intensity from a sample of the fluorocarbon Polytetrafluoroethylene (PTFE) produced by the stand-off system at the two wavelengths. PTFE which is more commonly known as "Teflon", was chosen due to its well known Raman bands, energy level structure and absorption bands.[48–50] PTFE has a prominent absorption band at approximately 161 nm attributed to an electronic transition and a strong Raman band at 731 cm^{-1} which was used here as the measure of Raman signal strength for the comparisons at 266 nm and 532 nm.[48,49] In the following, all mention of 'Raman intensity' refers to the intensity of the 731 cm^{-1} Raman band of PTFE.

4.1 Observed Raman Signal Dependence on Wavelength and Pulse Energy at 266 nm and 532 nm

The theory described in Section 2.1 and Section 2.2 suggests that the Raman intensity scattered from a sample is linearly dependent on incident pulse energy, and depends inversely to the fourth power of the wavelength. In addition, pre-resonance can result in further signal enhancement if a wavelength is nearly resonant with an electronic transition. By either, holding all other parameters constant, or correcting for components wavelength response, experiments were performed where the incident pulse energies at two different wavelengths were varied in order to confirm that Equation (2.5.1) is valid for this stand-off Raman system.

A 1064 nm Nd:YAG laser was frequency doubled to produce light at 532 nm or frequency quadrupled to produce 266 nm light. As both are harmonics of the fundamental 1064 nm laser radiation, both wavelengths have the same temporal pulse characteristics. When operating in 266 nm mode, an additional 266 nm mirror was always used to remove any unwanted 1064 nm and 532 nm radiation, ensuring pulse energy readings from a laser power meter accurately measured the 266 nm radiation. The 266 nm radiation was incident on a PTFE sample approximately 50 cm away. Two 266 nm lenses each with a focal length of 5 cm, were then used to collect the scatter from the sample for delivery to the spectrometer. The first lens was placed a focal length away from the sample to collect and collimate the scattered light. The collimated beam then passed through a 266 nm edge filter to remove the elastic Rayleigh scatter, with the transmission focused by the second lens onto the entrance slit of the spectrometer. Collimation is necessary to ensure that the filter's extinction of the Rayleigh component was maximized. Inside the spectrometer, the light was spectrally separated by a UV diffraction grating which directed the light onto the ICCD camera.

Two adjustable apertures placed 40 cm apart were used as an alignment aid to ensure that the beam path at 532 nm was the same as that used at 266 nm. Both apertures were opened to the diameter of the laser beam, with the first placed near the laser aperture and the second just before the sample. These apertures ensured that the laser was incident on approximately the same spot on the sample whenever the system was changed from operating in 266 nm mode to 532 nm mode and vice versa. The experimental layout is shown in Figure 4.1.

After completing the 266 nm measurements, all the 266 nm optics and the UV diffraction grating were replaced with equivalent 532 nm components. The experiments involved operating the laser at different average beam powers, ranging from 2 mW up to 99 mW when in 266 nm mode, and from 100 mW up to 451 mW in 532 nm mode. At both wavelengths, the ICCD camera had a gate width of 8 ns, approximately the same size as the shortest pulse duration used, and had the on-CCD accumulation setting set to 10, resulting in the capture of 10 laser pulses over 1 second. For every measurement 30 frames were captured with the camera, which showed the Raman signal pulse emitted from the PTFE. The frame corresponding to the maxima of the pulse was exported for each experiment, then Raman intensity was recorded and plotted. An example of the Raman spectra recorded and the image on the CCD is shown in Figure 4.2, while Figure 4.3 shows the plot of Raman intensity at each pulse energy for both wavelengths.

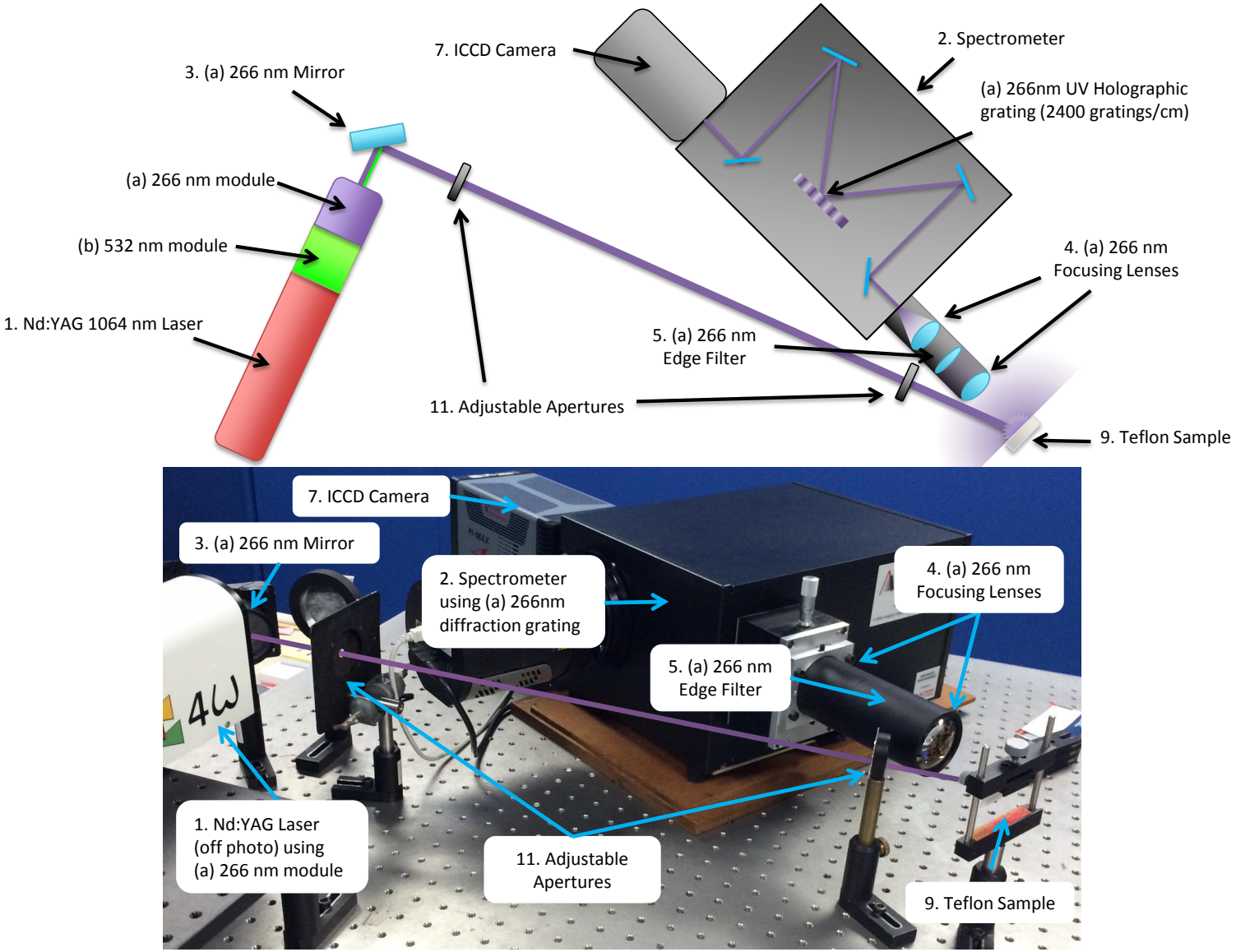

Figure 4.1: The first image shows a top down blueprint view for the experiment at 266 nm, while the bottom image shows the side on view photo of the same set up. The 532 nm experiment was set up in the same manner, but with the 266 nm equipment swapped out for the 532 nm equipment.

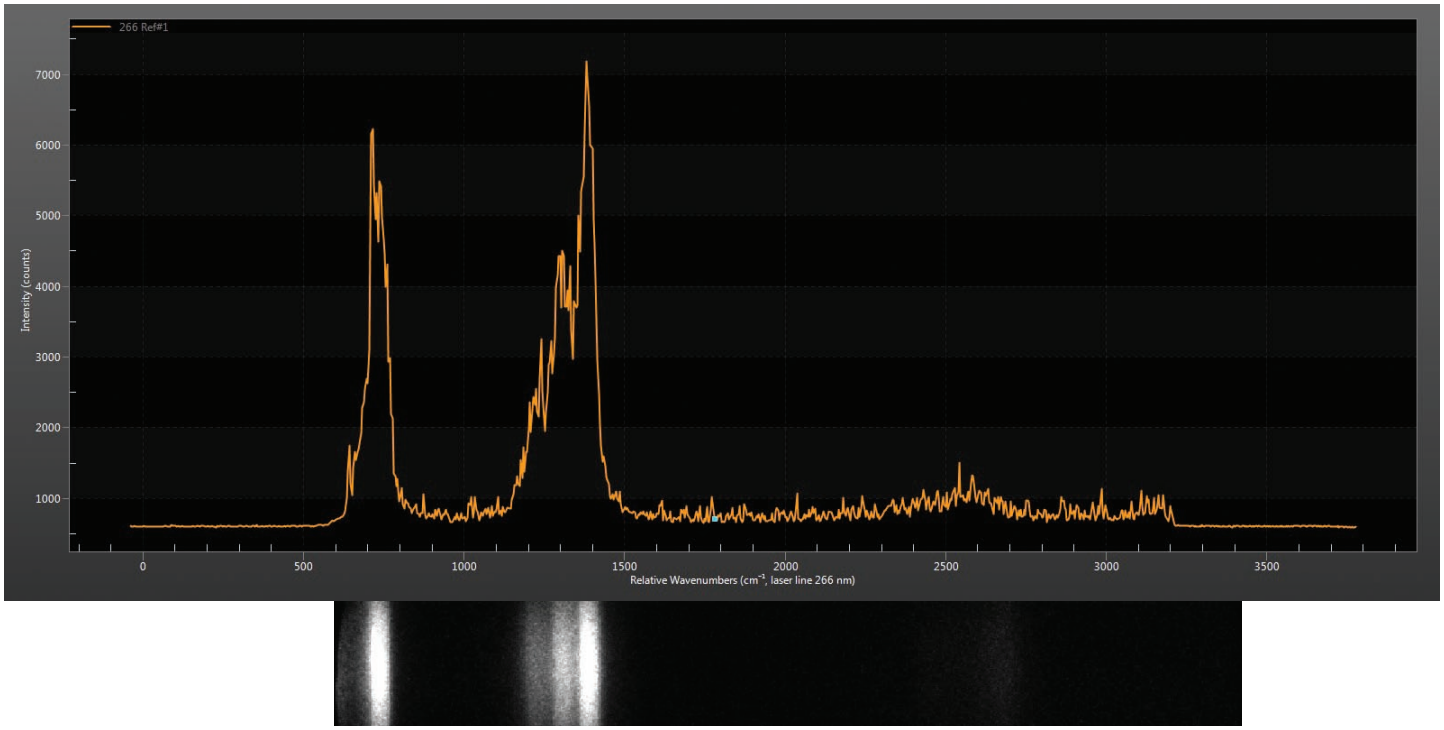

Figure 4.2: The top image shows a graph of the Raman photon count against the relative wavenumber from the 266 nm laser line, for one of the 266 nm distance tests. The bottom image shows the actual image on the CCD of the ICCD camera for the same test.

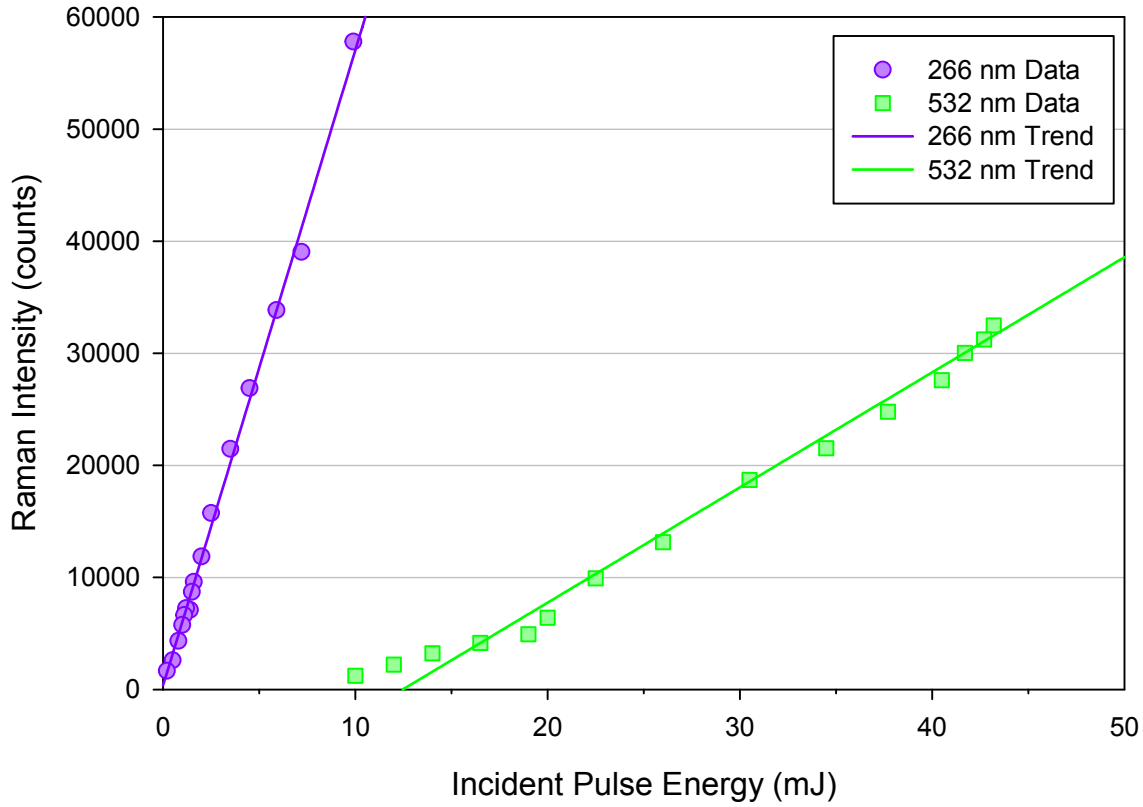

Figure 4.3: 532 nm and 266 nm Raman signal photon counts over incident pulse energy for PTFE.

As the results shown in Figure 4.3 indicate, the Raman signal intensity observed with this stand-off Raman system varies linearly with pulse energy and average beam power at both 266 nm and 532 nm. This is in good agreement with Equation (2.2.2) since these low incident intensities are not high enough to induce nonlinear Raman signal contributions in the sample, as described in Section 2.1. As a result it is therefore possible to use Equation (2.5.1) to predict the Raman signal that is observed at any given pulse energy at either 266 nm or 532 nm.

Using Equation (2.5.1) and the known frequencies of the electronic energy transitions and vibrational modes of PTFE, we can estimate the impact that wavelength and pre-resonance has on the Raman signal intensity at both 266 nm and 532 nm:[48,49]

$$\frac{I_{Raman}(266\text{ nm})}{I_{Raman}(532\text{ nm})} \propto \frac{(\nu_{266} \pm \nu_m)^4 \left[\frac{\nu_e^2+\nu_{266}^2}{(\nu_e^2-\nu_{266}^2)^2}\right]^2}{(\nu_{532} \pm \nu_m)^4 \left[\frac{\nu_e^2+\nu_{532}^2}{(\nu_e^2-\nu_{532}^2)^2}\right]^2} \approx 114. \tag{4.1.1}$$

Here ν_m is the vibrational frequency, ν_e is the frequency of the electronic transition, ν_{266} is the light frequency at 266 nm and ν_{532} is the light frequency at 532 nm. Ignoring other effects, it can be seen from Equation (4.1.1) that the combination of pre-resonance and the Raman signal dependence on excitation wavelength for PTFE, results in a Raman signal that is 114 times higher when 266 nm radiation is used for excitation instead of 532 nm

light. The measured dependence of Raman signal on incident pulse energy can be used to determine the number of Raman scattered photons produced as a fraction of the number of incident photons on the sample.

The number of incident photons, n_{in}, is related to the pulse energy, $\hat{H}_{in}$, through (4.1.2):

$$\hat{H}_{in} = n_{in} h\nu, \tag{4.1.2}$$

where h is Planck's constant and ν is the frequency of the light. Since the observed Raman signal depends linearly with incident pulse energy, Equation (4.1.2) can be combined with the CCD's quantum efficiency (QE_{CCD}), the diffraction grating efficiency ($QE_{Grating}$), and the edge filter efficiency (QE_{Filter}), all shown in Table 4.1, to determine the total number of Raman photons detected, n_{out}, over the number of incident photons, n_{in}, with the total ratio being

$$n_{ratio} = \frac{n_{out}}{n_{in}} \times QE_{CCD} \times QE_{Grating} \times QE_{Filter}. \tag{4.1.3}$$

Applying the total ratio of Raman photons that make it through the system found through Equation (4.1.3) to both 266 nm and 532 nm cases, and using the gradient of the best linear fit from Figure 4.3, we can deterimine the total output Raman intensity difference between both wavelengths through

$$\frac{I_{Raman}(266\text{ nm})}{I_{Raman}(532\text{ nm})} \approx \frac{n_{ratio}(266)}{n_{ratio}(532)} \times \frac{\nu_{266}}{\nu_{532}} \approx 53.8 \times 2 \approx 108, \tag{4.1.4}$$

which is in good agreement with the theoretical value of 114, as shown in Equation (4.1.1).

4.2 Observed Raman Signal Dependence on Accumulation Time for 266 nm and 532 nm Wavelengths

The quantum efficiency of a CCD at a given wavelength gives the fraction of incident photons that are detected. If a CCD has a quantum efficiency of 50%, then for every two photons that reach the CCD, only one will be recorded on average. In addition to the quantum efficiency, the photon counts detected by the CCD will also depend on the length of time the photons fall on the detector. Therefore, increasing the accumulation time will produce a greater Raman signal. The PI-MAX4 camera used here is a sensitive high performance detector that allows the camera to be gated allowing photon counts to be accumulated for a desired exposure time.

With increasing CCD accumulation time, a proportional increase in Raman signal photon count should be observed. To confirm this, the same set up described in Section 4.1 was used, which is shown in Figure 4.1. However, here the power was kept constant at

13 mW for the 266 nm laser and at 422 mW for the 532 nm laser. The CCD accumulation time was then varied, from 1 pulse duration up to 25 pulses for the 266 nm case, and from 1 pulse duration up to 100 pulses for the 532 nm set up. Results were recorded in the same manner as the previous experiment, with 30 frames being recorded and the frame corresponding to the pulse maxima was exported, with the 731 cm^{-1} Raman peak used for comparison. At both wavelengths the Raman signal obtained with this system is proportional to CCD accumulation time as shown in Figure 4.4.

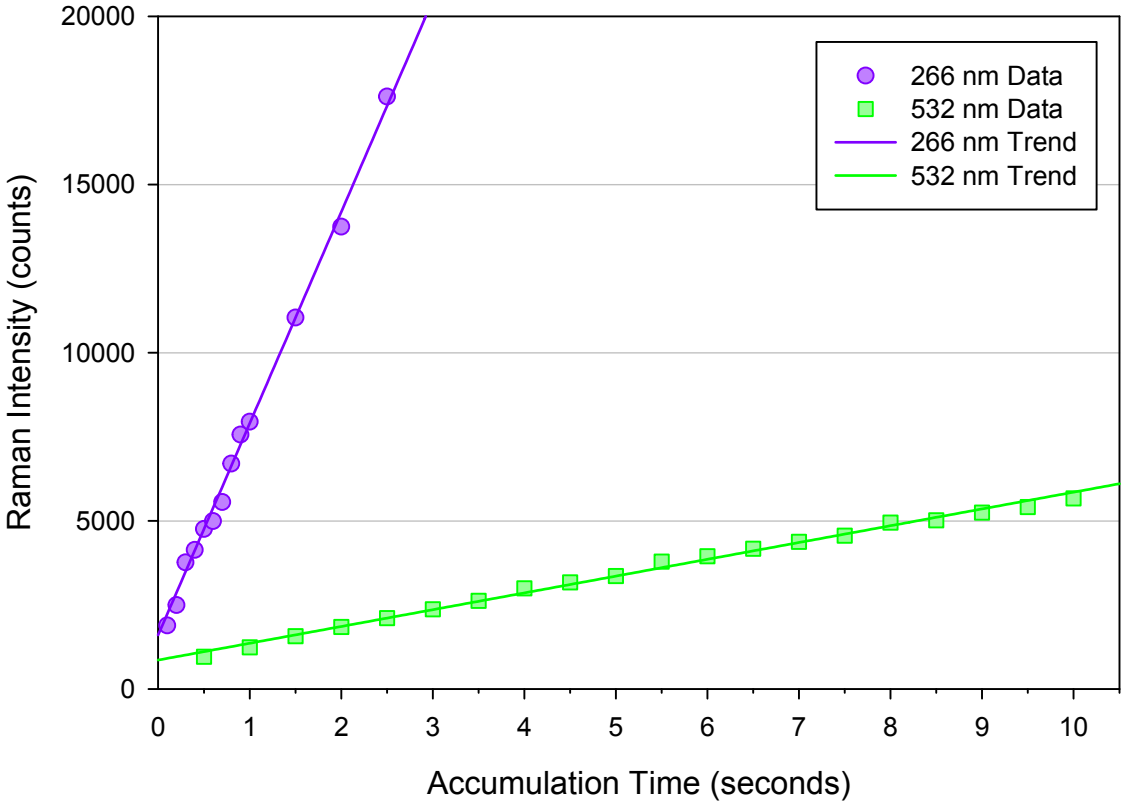

Figure 4.4: 532 nm and 266 nm Raman signal for PTFE over increasing on-CCD accumulation. The laser had a pulse energy of 42.2 mJ at 532 nm and the camera's intensifier set to 1% gain, while at 266 nm the laser had a pusle energy of 1.3 mJ while the camera's intensifier was set to 100% gain.

4.3 Observed Raman Signal Dependence on Sample Distance for 266 nm and 532 nm Wavelengths

One of the key figures of merit for a stand-off Raman system is the maximum distance at which it can detect substances. Here we determine the detection range of the Raman system used for the work in this thesis at both 266 nm and 532 nm. Consideration of Equation (2.4.2) in Section 2.4 suggests that, theoretically, the Raman signal intensity should depend inversely with the square of the sample distance. Therefore, doubling the

sample distance will result in a four fold drop in the detected Raman intensity. In order to use Equation (2.4.2) to estimate the maximum detection range it is important to confirm that signal observed with this actual Raman system displays this dependence on distance.

To determine this, the system was configured with the collection optics mounted on a translation stage to allow it to be moved with respect to the illuminated laser spot on the PTFE sample as shown in the experimental layout in Figure 4.5. Each time the collection optics were moved, they were realigned to ensure optimal focussing into the spectrometer through the coupled fibre. The experiment was performed at both 266 nm and 532 nm using optical elements appropriate for the particular incident wavelength used. This simulated moving the reference sample of PTFE while keeping the incident power density and spot size on the sample constant at all times.

With the 266 nm excitation, the distance between the PTFE sample and the collection optics was varied from 0.3 m up to 1 m away in steps of 0.05 m. When the system was configured with 532 nm excitation, the distance between sample and collection optics was varied from 0.3 metres up to 0.8 metres. At this wavelength, the Raman signal would fall to such low levels for distances greater than 0.8 m that it could not be measured from the noise. This noise that was observed at 532 nm but not at 266 nm was in all likelihood due to fluorescence.

For these experiments, the laser was operated at a constant average power of 72 mW over all distances when configured for 266 nm. When set up to for 532 nm it was necessary to use a higher constant average power of 620 mW because of the weaker Raman signals observed at large sample to collection optics distances. As the laser's repetition frequency was 10 Hz this corresponds to single pulse energies of 7.2 mJ at 266 nm and 62 mJ at 532 nm. For measurements at all distances the ICCD camera gate width was set to 8 ns, which is approximately the same as the laser pulse duration. The CCD accumulation was set to 10 pulses, so that the measurement of a single frame took 1 second. At each distance 30 frames were captured with the camera and examining these allowed the Raman signal from the PTFE sample to be displayed. The frame corresponding to the maxima of the emission pulse was then used as the Raman signal intensity measurement at that distance. These measurements are shown in Figure 4.6 and in Figure 4.7.

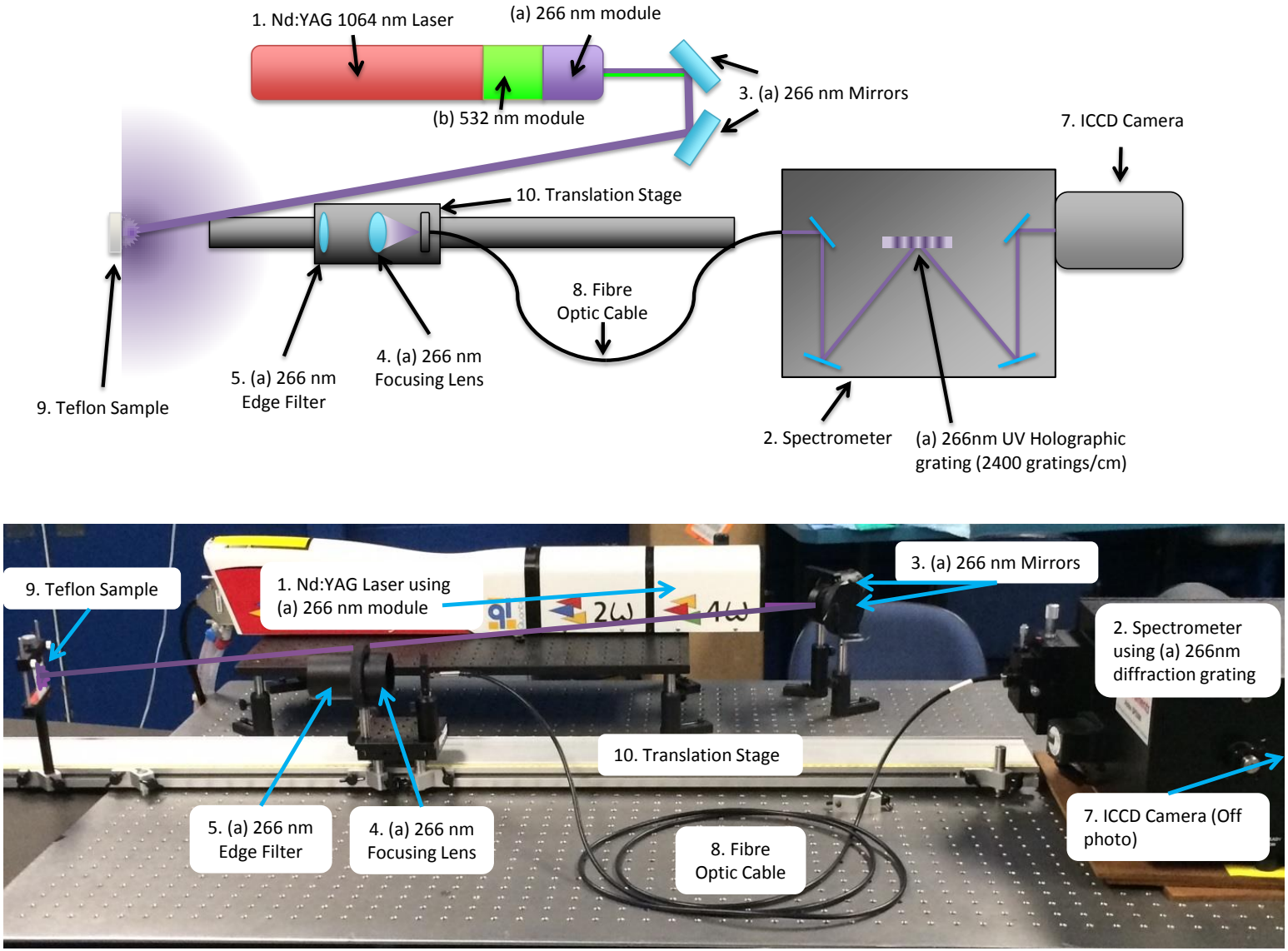

Figure 4.5: The first image shows a top down blueprint view for the experiment at 266 nm, while the bottom image shows the side on view photo of the same set up. The 532 nm experiment was set up in the same manner, but with the 266 nm equipment swapped out for the 532 nm equipment.

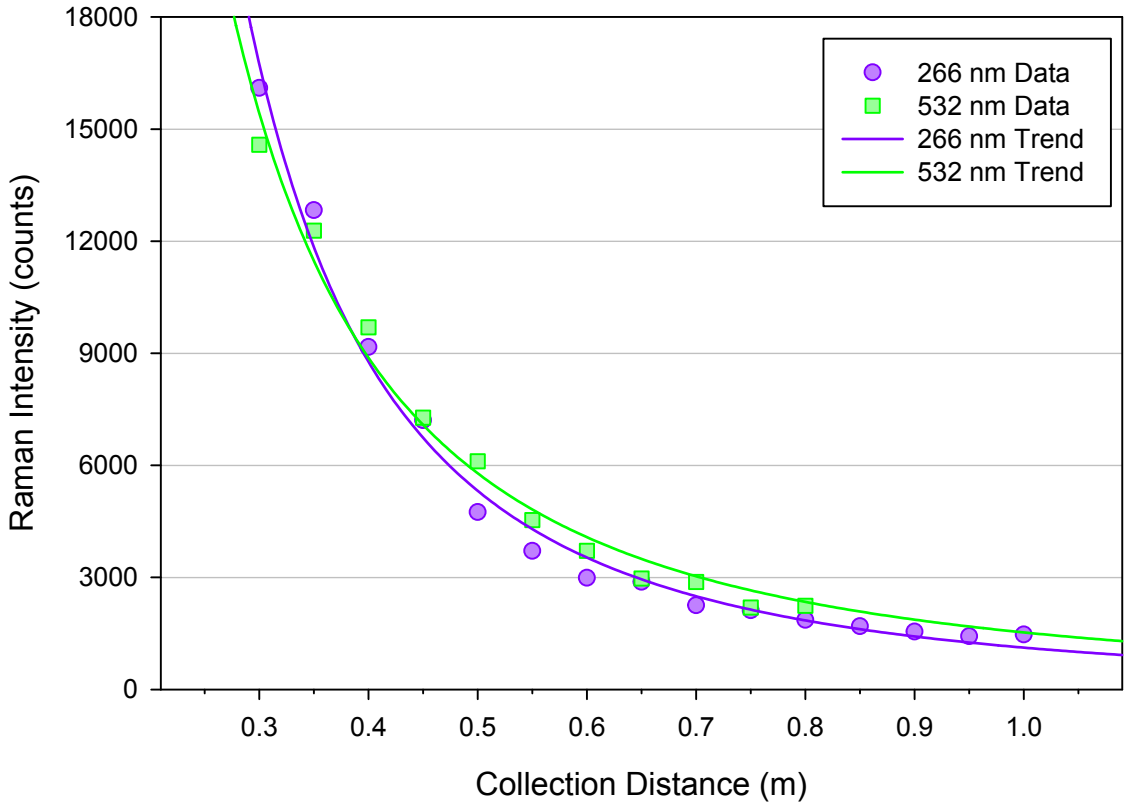

Figure 4.6: 532 nm and 266 nm Raman signal for PTFE over a range of collection distances.

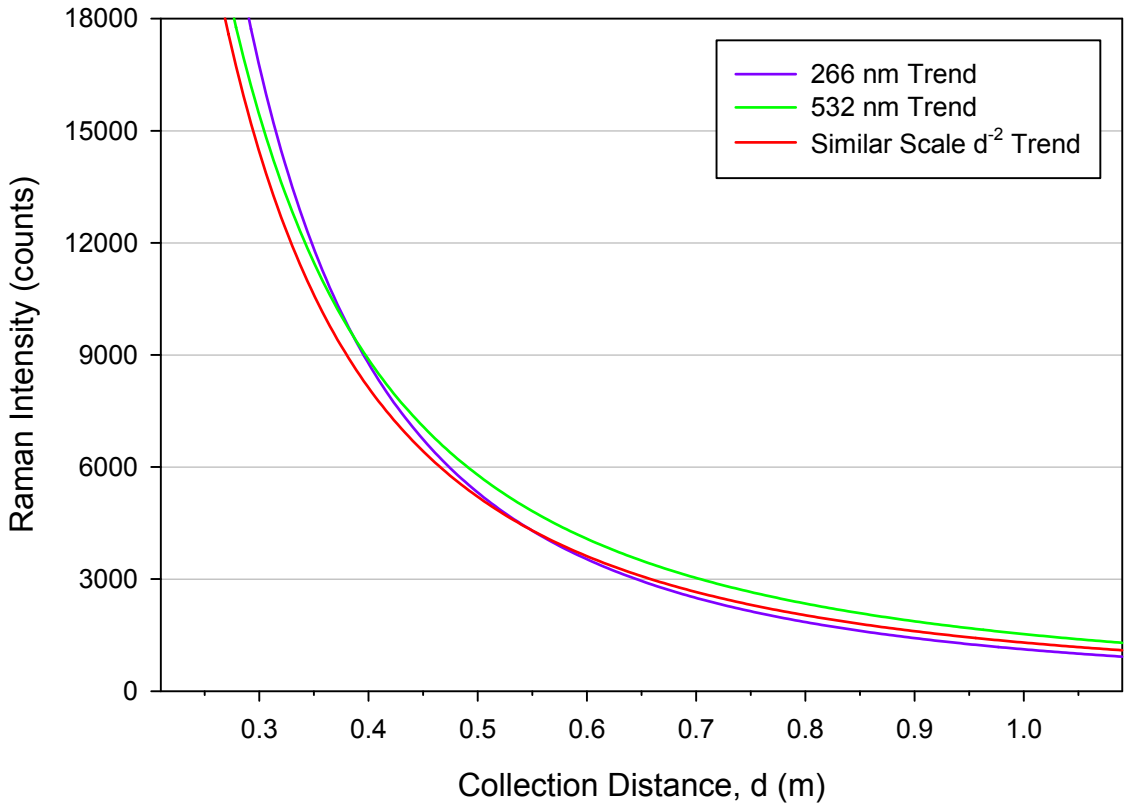

Figure 4.7: 532 nm and 266 nm Raman signal for PTFE over a range of collection distances, d, also showing a reference plot of d^{-2} at a similar scale.

As seen from Figure 4.6 and more clearly displayed in Figure 4.7, the results for both

the 266 nm and 532 nm experiments agree well with an inverse square law dependence of Raman signal on sample distance. This is as expected from the theory, since Raman scattering can generally be accurately modelled as an isotropic process regardless of excitation wavelength. An interesting thing to note about these results is that the Raman signal observed for the two different excitation wavelengths was approximately the same for equivalent sample locations despite the much higher pulse energy of the 532 nm laser. Therefore, even though the 62 mJ input pulse energy at 532 nm contained nearly 20 times more photons than the 7 mJ input pulses at 266 nm, each produced approximately the same number of Raman photon counts at the detector. Using this approximately equal signal at both wavelengths, along with Equation (4.1.2) and Equation (4.1.3), a similar approach can be followed as in Section 4.1 to find the ratio of photons that make it through the system at each wavelength:

$$\frac{I_{Raman}(266\text{ nm})}{I_{Raman}(532\text{ nm})} \approx \frac{n_{ratio}(266)}{n_{ratio}(532)} \times \frac{\nu_{266}}{\nu_{532}} \approx 43 \times 2 \approx 86, \tag{4.3.1}$$

which is not far from the theoretical value of 114 shown in Equation (4.1.1) considering this experiment was not designed for this specific comparison.

4.4 Observed Raman Signal Dependence on Incident Irradiance for 532 nm and 266 nm Wavelengths

While Equation (2.1.7) depends on many factors, such as incident power or energy, it is interesting to note that at low irradiances that the Raman signal does not depend on the incident energy density or radiant exposure of the illuminated spot on the sample. From an eye safety perspective this is significant since the safe exposure level, the MPE, is a measure of energy density. Therefore, high energy or power incident beams that produce intense Raman signals may still be used as long as the beam energy is spread over a significantly large area. However experimentally, there will be limits as to how large the incident beam can be before the detected Raman signal is affected. In this section, the dependence of the observed Raman signal from a PTFE sample, on the incident irradiance is investigated at both 266 nm and 532 nm. The experimental layout is shown in Figure 4.8, with a beam expander used to collimate the laser beam to a diameter of 20 mm before passing through a lens that focuses the light upon the sample. The focusing lens was attached to a translational stage, which moved towards and away from the sample, allowing the incident beam diameter and therefore, radiant exposure and irradiance, upon the sample to be varied. The resulting light was then collected in the same manner as described previously in Section 4.1. The results are shown in Figure 4.9.

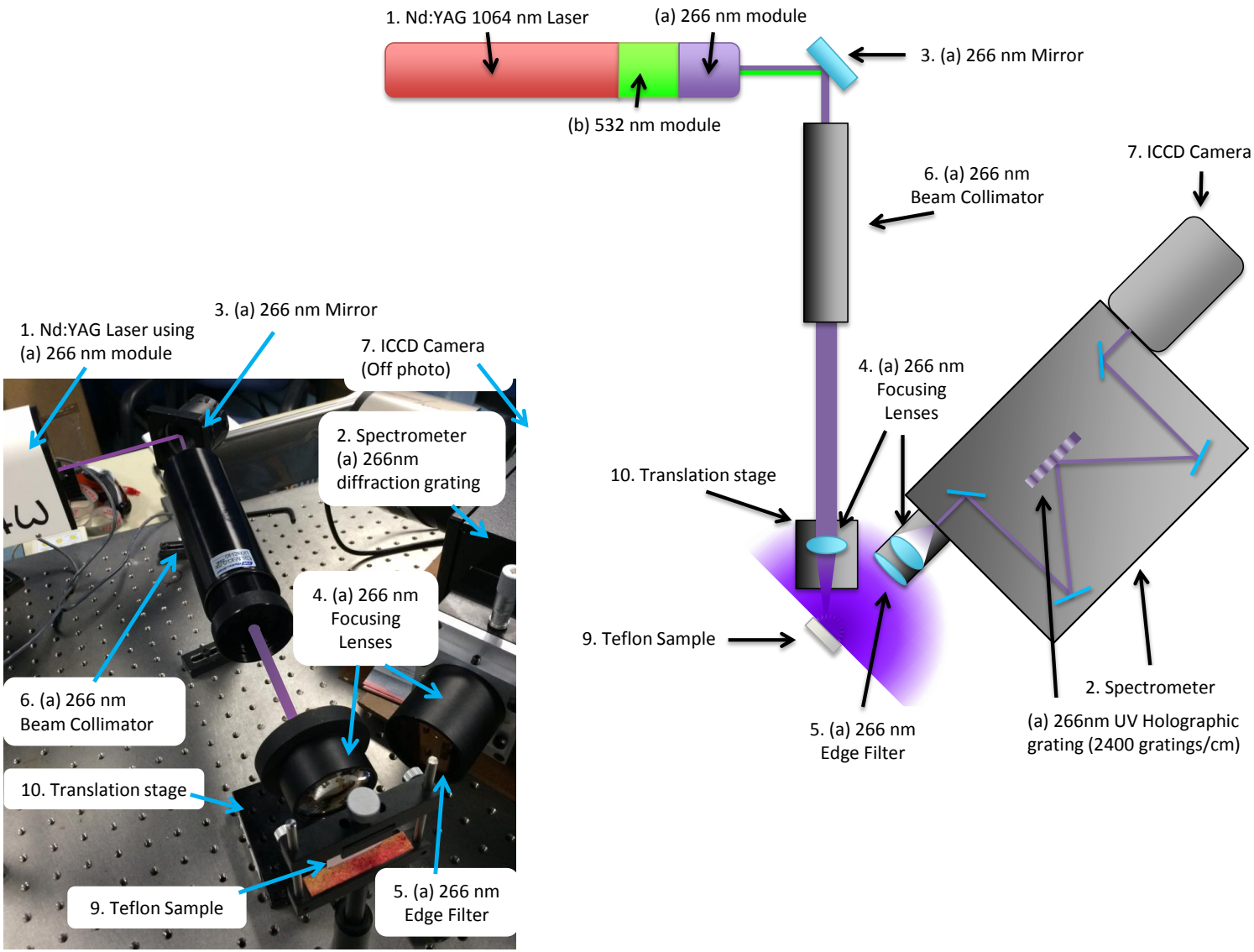

Figure 4.8: The first image shows a top down blueprint view for the experiment at 266 nm, while the bottom image shows the side on view photo of the same set up. The 532 nm experiment was set up in the same manner, but with the 266 nm equipment swapped out for the 532 nm equipment.

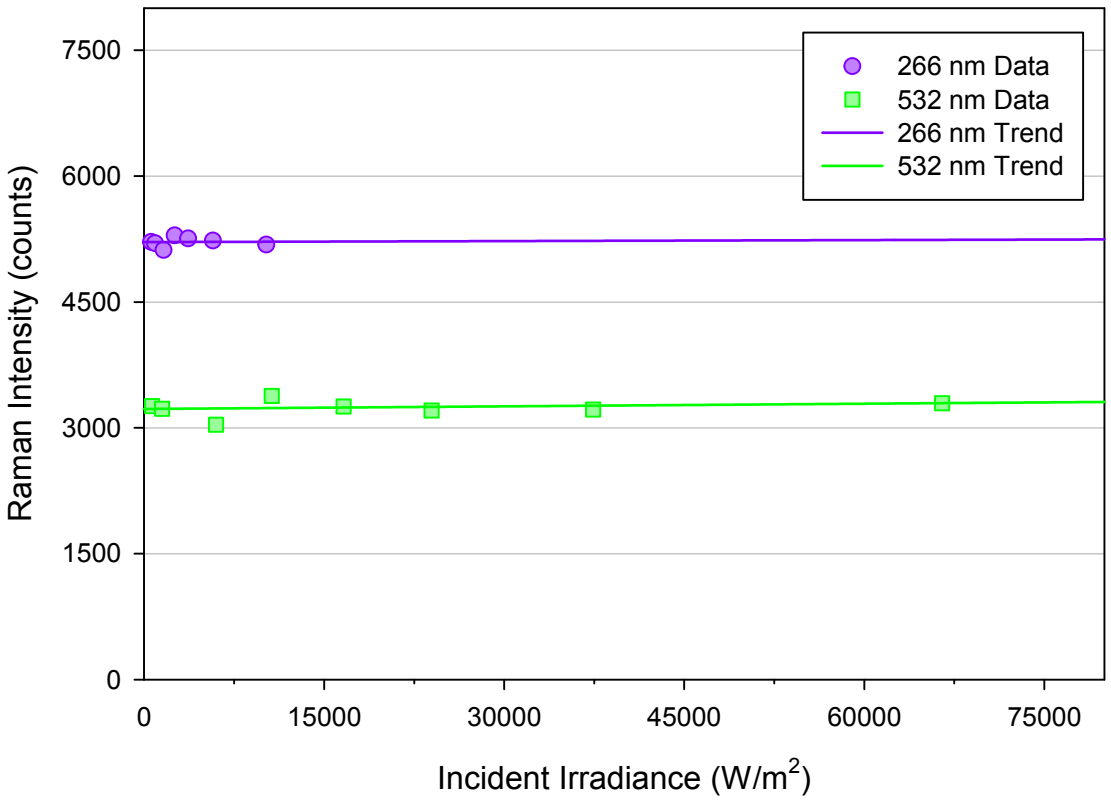

Figure 4.9: 266 nm and 532 nm Raman signal for PTFE over irradiance from the incident laser.

Figure 4.9 shows that the detected Raman signal is unaffected by the change in the incident irradiance at the sample. As a result, it is possible to obtain larger Raman signal intensities with this Raman system, by increasing the beam energy if the beam diameter is increased to keep the irradiance below the MPE. As described in Section 4.1, an increase in allowable laser energy increases the overall detection range for the stand-off Raman system, so this makes it possible to increase the range while still maintaining eye-safe conditions. A practical limit to how large the laser beam can be is the sample size itself. There is no advantage in having a beam diameter that exceeds the physical size of the sample. As many common explosive devices are several centimetres in length, width and height, this would suggest that beam diameters of this scale are suitable for use with this technique for maximising stand-off Raman range for explosive detection.

Similar to the approach in Section 4.3, we can compare the overall efficiency of producing Raman photons at 266 nm and 532 nm. Using Equation (4.1.2) and substituting in appropriate values for incident pulse energy and from Table 4.1, the ratio of Raman photons generated at the sample is

$$\frac{I_{Raman}(266\text{ nm})}{I_{Raman}(532\text{ nm})} \approx \frac{n_{ratio}(266)}{n_{ratio}(532)} \times \frac{\nu_{266}}{\nu_{532}} \approx 53 \times 2 \approx 106, \tag{4.4.1}$$

which is similar to the theoretical value of 114 shown in Equation (4.1.1), and close to the experimental value of 108 found in Section 4.1.

4.5 Demonstration of Stand-off Raman Signals with Safe Radiant Exposures

The experiments described in Sections 4.1, 4.2, 4.3, and 4.4 demonstrate that the dependence of the detected Raman signal, observed with this stand-off Raman system, on various incident beam parameters agrees well with the theoretical considerations discussed in Chapter 2. This suggests that more optimal Raman signal levels will be obtained with shorter incident wavelengths. Combining this with the higher MPEs at UV wavelengths suggests that it should be possible to practically realize a UV stand-off Raman system that uses incident laser radiation at emission levels below the MPE.

Several experiments were conducted with various materials to determine if stand-off Raman signals are detectable with a UV laser emission levels below the MPE. All experiments used the 266 nm UV laser, with a 1 second exposure on the sample equivalent to 10 pulses. If an angular subtense of 1.5 mrad is assumed, the relevant MPE at 266 nm for a 1 s exposure with an 8 ns pulse duration at a repetition rate of 10 Hz is 3 J/m^2 (Table 3.1 and Figure 3.3). In all of the following experiments, the laser beam is collimated to a diameter of 20 mm, which restricts the pulse energy to approximately 0.94 mJ per pulse if the beam radiant exposure is to remain below the MPE. To ensure that the MPE is not exceeded, the laser was operated with a pulse energy of approximately 0.9 mJ per pulse. The experimental layout for all the following experiments is shown in Figure 4.10.

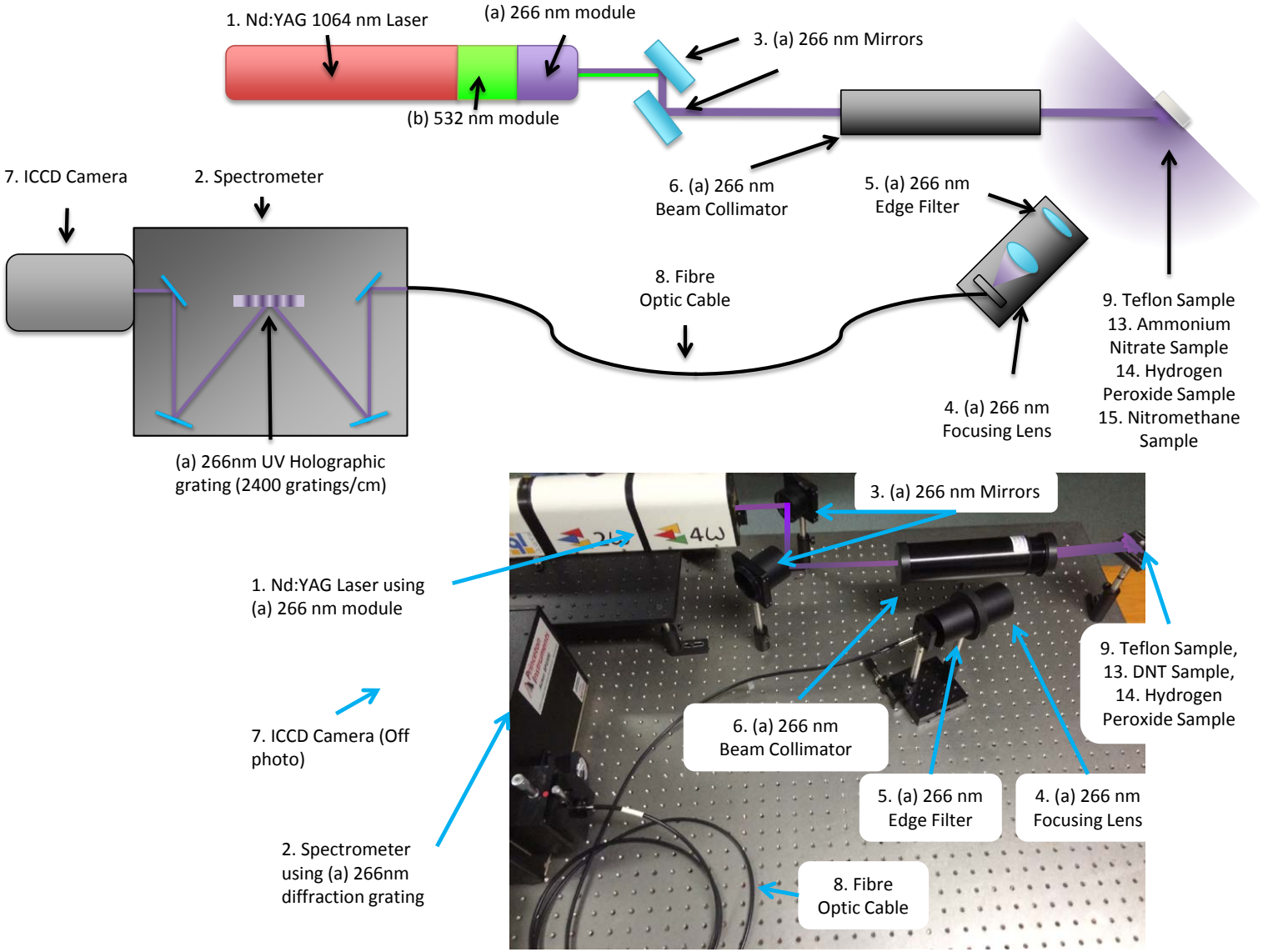

Figure 4.10: The first image shows a top down blueprint view for the experiment at 266 nm, while the bottom image shows the side on view photo of the same set up. The 532 nm experiment was set up in the same manner, but with the 266 nm equipment swapped out for the 532 nm equipment.

4.5.1 Stand-off Raman Detection of PTFE with Radiant Exposures Less than the MPE

A stand-off Raman system with a stand-off distance of 30 cm was constructed to detect PTFE using 266 nm incident radiation with radiant exposures less than the MPE. The resulting Raman spectrum for the experiment is shown in Figure 4.11.

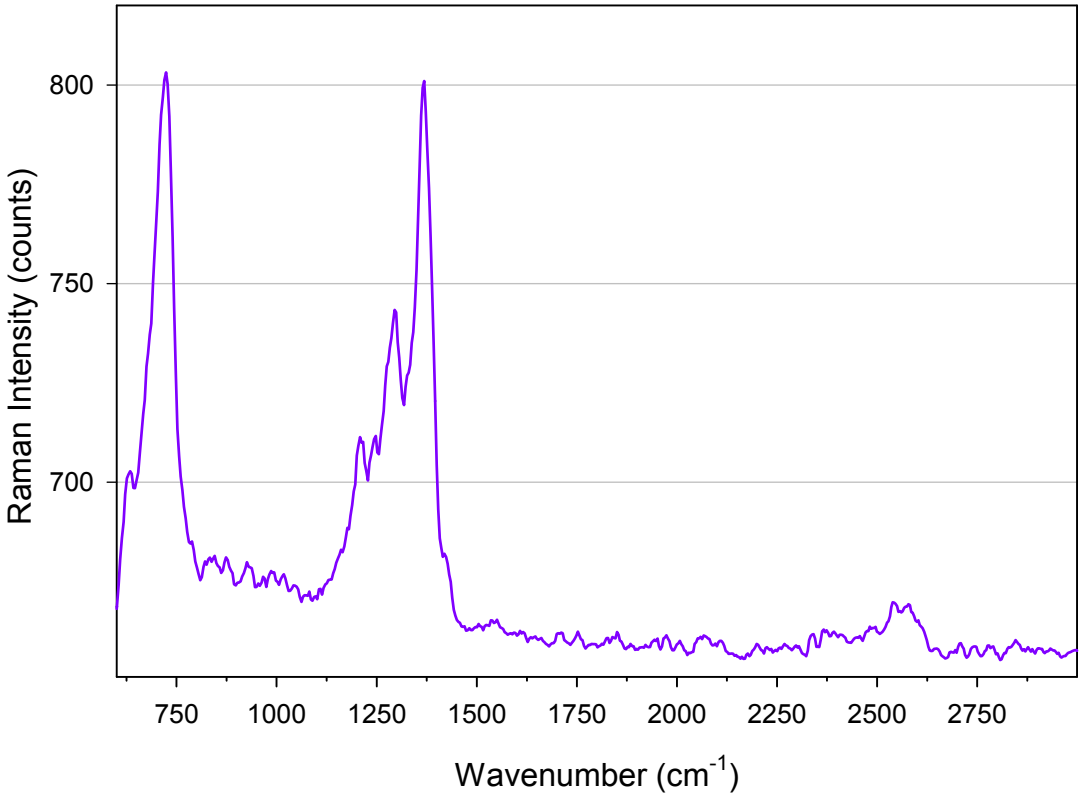

Figure 4.11: 266 nm stand-off Raman spectrum of PTFE, collected 30 cm away with ten 0.9 mJ pulses, being below the MPE of 0.94 mJ pulses.

Quite clearly, even at radiant exposures below the MPE, it is possible to obtain sufficiently strong Raman signals to allow identification of the PTFE sample. While the 30 cm stand-off distance used in this demonstration is not large, it is clear that a high signal to noise ratio is possible even with a detection time of 1 second. Therefore, by extrapolation of the data shown in Figure 4.11, it is possible to estimate the maximum possible collection distance achievable with this specific system by using its proven linear dependence of Raman signal on pulse energy (Section 4.1). As the detected Raman photon count of the 731 cm^{-1} band is approximately 800 counts at a sample distance of 30 cm, the maximum stand-off detection range for PTFE with a single pulse energy of 0.94 mJ, a beam diameter of 20 mm, can be calculated from Equation (2.4.2) to be approximately 8.4 metres. At this distance the detected Raman photon count falls to 1 count. Further increase to the maximum detection distance can be achieved through two methods, expanding the

excitation beam diameter, and/or increasing the area of the collection optics (eg essentially increasing the numerical aperture of the collector). As discussed in Section 4.4, expanding the excitation beam diameter allows the pulse energy to be increased, resulting in a linear increase in Raman intensity, without increase in radiant exposure.

For example, Table 4.2 lists the calculated maximum pulse energies that can be used for particular beam diameters, and the corresponding maximum detection distances of PTFE for this particular 266 nm stand-off Raman system.

Table 4.2: Maximum safe pulse energy and corresponding maximum detection range for varying beam sizes on PTFE using the 266 nm laser system.

Beam Diameter (mm)	Max Eye-safe Pulse Energy (mJ)	Max Detection Range (m)
7	0.12	3
10	0.24	4.2
20	0.94	8.5
50	5.89	21
100	23.5	42

Further increase of the maximum detection range is possible by the increasing the size of the collection optics. The Raman scattered light was collected with a 6 cm diameter lens in all experiments described in this thesis. However, in many existing stand-off Raman systems, detection at larger distances commonly involves the use of telescopes with diameters of 20 cm or larger. This will greatly increase the Raman signal detected as the area of collection is much larger, and thus further the maximum detection range.

4.5.2 Stand-off Raman Detection of Ammonium Nitrate with Radiant Exposures Less than the MPE

Ammonium nitrate is a white crystalline solid, with the molecular formula of NH_4NO_3, and is sometimes used in the production of homemade or improvised explosive devices.[34,51] Due to the availability of the substance, detection is important in areas that may be a potential target for the use of unauthorised explosive devices. A stand-off Raman experiment, similar to that described in Section 4.5.1, was performed with a radiant exposure below the MPE, however this time using ammonium nitrate as a sample. The collection distance between the sample and the collection lens was 15 cm, with the resulting Raman spectrum of ammonium nitrate shown in Figure 4.12.

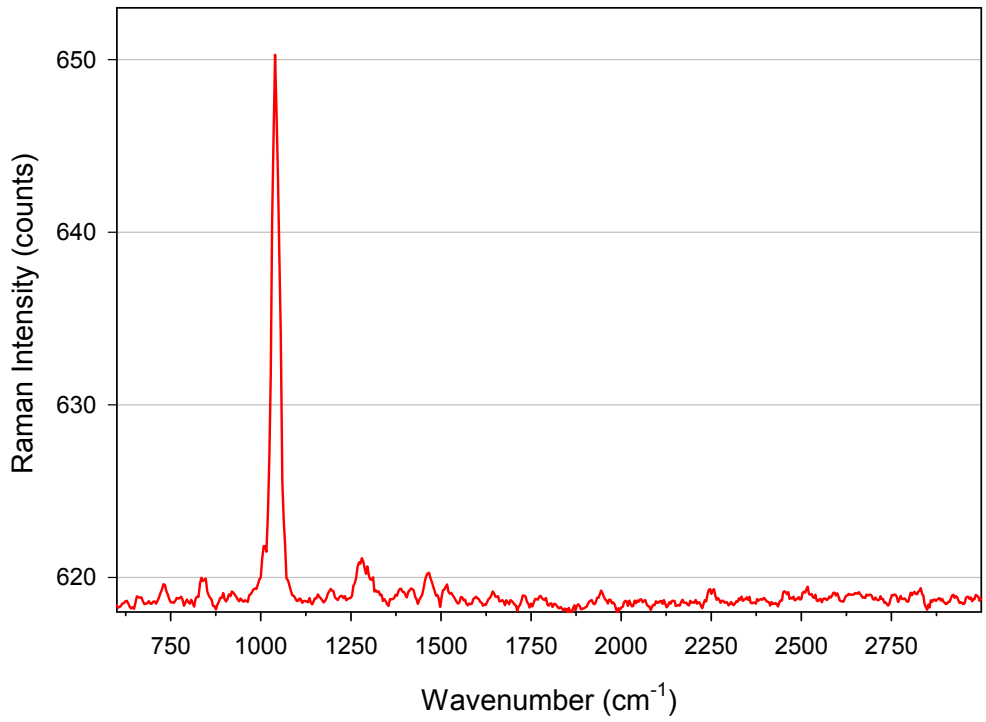

Figure 4.12: 266 nm stand-off Raman spectrum of Ammonium Nitrate, collected 15 cm away with ten 0.9 mJ pulses, being below the MPE of 0.94 mJ pulses.

Ammonium nitrate contains a Raman band at approximately 1043 cm^{-1},[34,40] which can be clearly seen in Figure 4.12, confirming that stand-off Raman detection of explosive devices using this material, is possible with this system at incident radiant exposures below the MPE. With the 1040 cm^{-1} Raman band showing approximately 650 Raman photon counts detected at this collection distance of 15 cm, we can use Equation (2.4.2) to extrapolate the maximum detection range of this system to be approximately 4 metres. Further detection range is then available through the use of larger collection optics, and/or by expanding the diameter of the incident beam as discussed in Section 4.5.1. A number of extrapolated maximum Raman detection ranges at varying beam diameters for ammonium nitrate are shown in Table 4.3.

Table 4.3: Maximum safe pulse energy and corresponding maximum detection range for varying beam sizes on NH_4NO_3 using the 266 nm laser system.

Beam Diameter (mm)	Max Eye-safe Pulse Energy (mJ)	Max Detection Range (m)
7	0.12	1.4
10	0.24	2
20	0.90	4
50	5.89	10
100	23.5	20

4.5.3 Stand-off Raman Detection of Nitromethane with Radiant Exposures Less than the MPE

Nitromethane is a liquid compound with the molecular formula CH_3NO_2, containing explosive properties. While highly explosive on its own, it is often mixed with ammonium nitrate to form dangerous homemade explosive devices, such as those used in the terrorist attack on Oklahoma city in 1995 killing 168 people.[52] With the danger this chemical presents for improvised explosive devices, it is of particular interest to ensure it can be detected at range. Using the setup described in Section 4.5, a stand-off Raman experiment was carried out with radiant exposures from the incident laser below the MPE. The collection distance between the nitromethane and collection optics was 10 cm, with the resulting Raman spectrum shown in Figure 4.13.

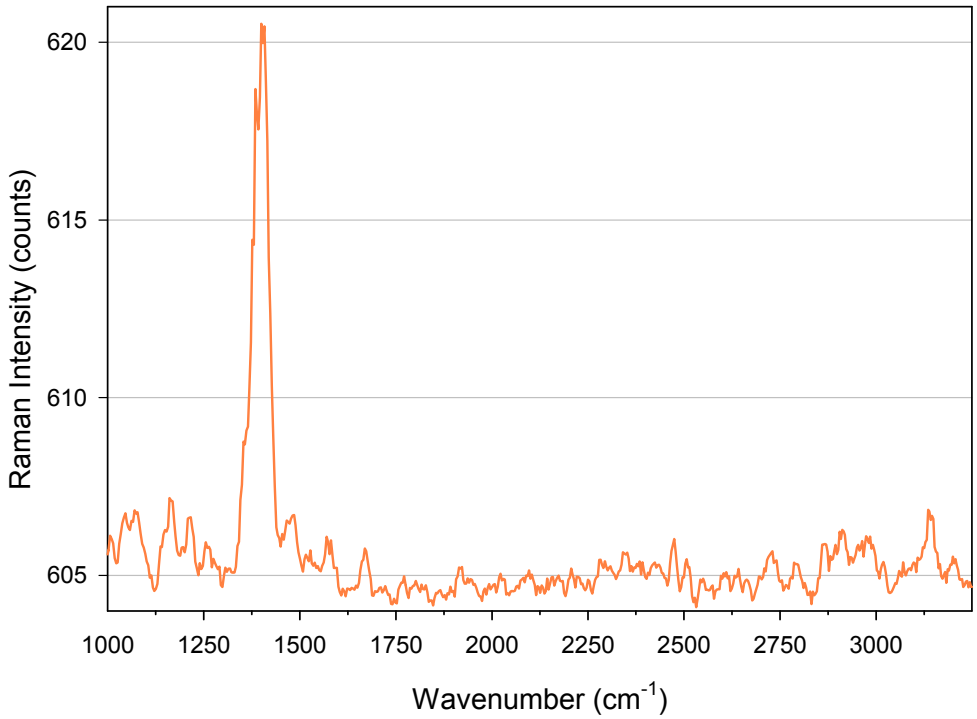

Figure 4.13: 266 nm stand-off Raman spectrum of Nitromethane, collected 10 cm away with ten 0.9 mJ pulses, being below the MPE of 0.94 mJ pulses.

Nitromethane has two strong Raman bands at approximately 1378 cm^{-1} and 1400 cm^{-1}, which can be seen in Figure 4.13.[53] The 1400 cm^{-1} Raman band contained approximately 620 counts with the 10 cm collection distance, which can be extrapolated to be a maximum detection range of approximately 2.5 metres by using Equation (2.4.2). As previously discussed in this chapter, further detection distance is acheivable by expanding the diameter of the incident beam, and/or using collection optics with a larger diameter. As demonstrated in previous sections, several extrapolated maximum Raman detection ranges for nitromethane at different beam diameters are shown in Table 4.4.

Table 4.4: Maximum safe pulse energy and corresponding maximum detection range for varying beam sizes on CH_3NO_2 using the 266 nm laser system.

Beam Diameter (mm)	Max Eye-safe Pulse Energy (mJ)	Max Detection Range (m)
7	0.12	0.7
10	0.24	1
20	0.90	2
50	5.89	5
100	23.5	10

4.6 Conclusion

Throughout this chapter, the theory from Chapter 2 was experimentally investigated as discussed in Section 4.1 through to Section 4.4, confirming that the system behaved as the theory suggested. Section 4.1 discussed the Raman signal's theoretical dependence on pre-resonance, incident wavelength, and incident energy, while Section 4.2 showed the accuracy of the Raman signal's theoretical dependence on CCD acquisition time. The theoretical dependence on Raman signal due to varying collection distance was confirmed in Section 4.3, while the effect on Raman signal due to changing incident radiant exposure on a sample was shown to be valid in Section 4.4.

These experimental results show that this Raman system used here behaved as theoretically expected, experiments were described in Section 4.5 to obtain Raman signals were obtained with safe radiant exposures using optimal parameters. As Section 4.5 shows, Raman signals are indeed achievable with the 266 nm laser system below the safe level of emission, with detection achieveable up to 40 metres away. No Raman signals were detectable below the relevant safe level of emission using the 532 nm system, even with short collection distances in the order of centimetres. This demonstrates that the 266 nm system and other UV Raman systems, can acheive stand-off Raman detection below the MPE, whereas visible Raman systems are unable to achieve this.

Table 4.2 in Section 4.5.1 shows the maximum ranges obtained with certain beam diameters at which the 266 nm system can achieve a Raman signal from a sample of PTFE. This table shows that with a beam diameter of 100 mm, a maximum Raman detection range of 42 metres is achieveable with this specific 266 nm system, based on the experimental results involving PTFE. Section 4.5.2 and Section 4.5.3 involved stand-off Raman experiments under the MPE using two materials commonly used separately and combined together in improvised and homemade explosive devices, being ammonium nitrate and nitromethane. Both of these materials provided a detectable Raman signal from the stand-off Raman experiments conducted below the MPE, confirming that stand-

off UV Raman is achievable under the safe limit for the detection of common materials used in explosives.

Summary

5

This thesis highlights the importance of developing rapid means of explosives detection in order to adequately counter their increasing use in terrorist attacks as witnessed over the past 10 years. In Section 1.2, several of the more promising explosive detection methods were described including ion mobility spectroscopy, chromatography, infrared spectroscopy, terahertz spectroscopy, and Raman Spectroscopy. Raman spectroscopy is a non-contact optical technique that is particularly suited to explosives detection at distance, since the technique can accurately detect materials at distances over several hundred meters away without damage to the sample. Unfortunately, to achieve such impressive detection ranges, stand-off Raman spectroscopy typically requires the use of excitation lasers with radiant exposures that are significantly above the damage threshold of biological tissue found in the human eye and skin. This risk of possible eye or skin injury through exposure to the laser beam is limiting the use of the stand-off Raman technique in public places.

The principal aim of this thesis was to determine the maximum detection range that could be achieved with a stand-off Raman system with laser emission that was safe in that it was incapable of damaging the eye or skin. This is possible since both the detection range and injury risk depend on beam parameters such as wavelength, pulse energy, beam diameter, and others. Chapter 2 investigated theoretically the dependence of Raman signal on laser parameters, such as wavelength and energy of a laser incident upon a sample, the distance between a sample and the collection optics, and also on material related effects such as proximity to absorption resonances. A key result of this analysis was that superior Raman signals can be expected at UV wavelengths with the signal increasing when the pulse energy is increased. However, once the pulse energy exceeds a specific threshold, the MPE, then it becomes capable of injuring the eye or skin.

In Chapter 3 the safe threshold levels of laser emission were evaluated for beam parameters that are typical for the stand-off Raman application. This analysis showed that spectral windows exist in the UV and IR regions of the spectrum, where the eye and skin

are more resilient to laser induced injury and can therefore tolerate higher power densities than other regions of the spectrum. Combining the theoretical considerations of Chapter 2 and Chapter 3 suggests that stand-off Raman systems using lasers with wavelengths in the UV region of the spectrum will offer the greatest detection range, while still remaining safe and useable in public locations. To validate this, experiments are described in Chapter 4 that show the Raman signals obtained with actual stand-off Raman system at 266 nm and 532 nm behave as theoretical expected. In Section 3.1 and Section 4.1 it was shown that Raman signal intensities using UV excitation lasers at safe emission levels, are several orders of magnitude higher than Raman signal intensities resulting from a similar safe level of emission excitation laser at longer wavelengths. This is primarily because of the significant signal gains obtained in the UV because of the dependence of Raman scattering on wavelength as discussed in Section 2.1, in addition to signal gain through pre-resonance as discussed in Section 2.3.1. These gains at UV excitations allow Raman spectra to be obtained from a sample over a much larger distance, with the signal falling as the inverse square of the detector distance as experimentally shown in Section 4.3. This allowed the maximum operating range of the actual eye-safe 266 nm stand-off Raman system to be extrapolated for detecting the reference Teflon sample. For a beam diameter of 20 mm, it was found in Section 4.5.1 that the system could detect the sample up to a distance of 8.4 metres, when eye-safe pulse energies of 0.9 mJ were used.

In Section 4.4 it was shown that further increase in detection range is possible through increasing beam diameter. This section demonstrated experimentally that the Raman signal depends on pulse energy and not on the incident power density that falls upon the sample. Therefore, it is possible to increase the pulse energy and as a result increase the Raman signal, without impact on power density as long as the beam diameter is increased by an appropriate amount. This will result in a greater operating range without increasing the injury risk of exposure to the beam. In Section 4.5, experimental evidence is provided that shows that stand-off Raman system here can be used for detection of materials found in many explosives using 266 nm light at radiant exposures below the MPE. It was found that this system could detect ammonium nitrate at a distance of 0.15 m, with a maximum detection distance of 20 m available through increasing beam diameter. Nitromethane could be detected at 0.1 m, with an increase in beam diameter providing a maximum detection distance of 10 m.

This demonstrates that it is possible to use the Raman technique with accessible beams for explosives detection in public areas without risk of injuring operators or bystanders. Future research will focus on issues such as separating the desired signal from noise, such as the Raman signal and fluorescence resulting from packaging that may surround

the explosive material. This will allow the technique to detect deliberately concealed explosives and further extend the applicability of this promising eye-safe UV stand-off Raman method of detection.

References

[1] National Consortium for the Study of Terrorism and Responses to Terrorism (START). (2013). Global Terrorism Database [globalterrorismdb_1213dist.xlsx]. Retrieved from http://www.start.umd.edu/gtd.

[2] National Consortium for the Study of Terrorism and Responses to Terrorism (START). (2014). *Annex of Statistical Information - Country Reports on Terrorism 2013*. Tech. rep. April. 2014.

[3] M. H. Hicks, H. Dardagan, P. M. Bagnall, et al. *Casualties in civilians and coalition soldiers from suicide bombings in Iraq, 2003-10: a descriptive study*. **Lancet** 378 (2011), pp. 906–14. DOI: 10.1016/S0140-6736(11)61023-4.

[4] G. B. Kapur, H. R. Hutson, M. A. Davis, et al. *The United States Twenty-Year Experience With Bombing Incidents: Implications for Terrorism Preparedness and Medical Response*. **J. Trauma Inj. Infect. Crit. Care** 59.6 (2005), pp. 1436–44. DOI: 10.1097/01.ta.0000197853.49084.3c.

[5] J. S. Caygill, F. Davis, and S. P. J. Higson. *Current trends in explosive detection techniques*. **Talanta** 88 (2012), pp. 14–29. DOI: 10.1016/j.talanta.2011.11.043.

[6] D. S. Moore. *Recent Advances in Trace Explosives Detection Instrumentation*. **Sens. Imaging An Int. J.** 8.1 (2007), pp. 9–38. DOI: 10.1007/s11220-007-0029-8.

[7] A. Kanu, P. Dwivedi, M. Tam, et al. *Ion mobilitymass spectrometry*. **J. Mass Spectrom.** 43 (2008), pp. 1–22. DOI: 10.1002/jms.1383.

[8] G. A. Eiceman, Z. Karpas, and H. H. Hill Jr. *Ion Mobility Spectrometry*. 3rd Revise. CRC PRESS INC, 2013. ISBN: 9781439859971.

[9] H. Borsdorf, T. Mayer, M. Zarejousheghani, et al. *Recent Developments in Ion Mobility Spectrometry*. **Appl. Spectrosc. Rev.** 46.6 (2011), pp. 472–521. DOI: 10.1002/jms.1383.

[10] L. S. Ettre. *M.S. Tswett and the invention of chromatography*. English. **LC GC North Am.** 21.5 (2003), pp. 458–464,466–467.

[11] V. Arakelyan and K. Sakodynskii. *The contribution of gas chromatography to the identification of substances*. **Chromatogr. Rev.** 15.2-3 (1971), pp. 93–110. DOI: 10.1016/0009-5907(71)80015-7.

[12] E. Buxbaum. *Biophysical Chemistry of Proteins: An Introduction to Laboratory Methods*. 2011, pp. 147–162. ISBN: 9781441972507. DOI: 10.1007/978-1-4419-7251-4.

[13] B. C. Bohrer, S. I. Merenbloom, S. L. Koeniger, et al. *Biomolecule analysis by ion mobility spectrometry*. **Annu. Rev. Anal. Chem.** 1 (2008), pp. 293–327. DOI: 10.1146/annurev.anchem.1.031207.113001.

[14] P. W. Carr, D. R. Stoll, and X. Wang. *Perspectives on Recent Advances in the Speed of High Performance Liquid Chromatography*. **Anal. Chem.** 83.6 (2011), pp. 1890–1900. DOI: 10.1021/ac102570t.

[15] B. V. Malviya R, O. P. Pal, and P. K. Sharma. *High Performance Liquid Chromatography: A Short Review*. **J. Glob. Pharma Technol.** 2.5 (2010), pp. 22–26. DOI: 10.1234/jgpt.v2i5.208.

[16] P. Prévost, B. Stewart, and G. Kirchhoff. *The Laws of Radiation and Absorption: Memoirs by Prévost, Stewart, Kirchhoff, and Kirchhoff and Bunsen*. 1902. ISBN: 9781179164106.

[17] D. A. Burns. *Practical Spectroscopy, Volume 35: Handbook of Near-Infrared Analysis*. 3rd ed. CRC Press, 2007. ISBN: 9780849373930.

[18] B. Schrader. *Infrared and Raman Spectroscopy : Methods and Applications*. Wiley-VCH, 2008. ISBN: 9783527264469.

[19] B. H. Stuart. *Infrared Spectroscopy: Fundamentals and Applications*. 2004, p. 244. ISBN: 9780470854280.

[20] R. A. Spragg. *Encyclopedia of Spectroscopy and Spectrometry*. Elsevier, 2010, pp. 1199–1209. ISBN: 9780123744135. DOI: 10.1016/B978-0-12-374413-5.00088-9.

[21] P. W. Atkins and J. De Paula. *Elements of physical chemistry*. 6th ed. Oxford University Press, 2013. ISBN: 9780199608119.

[22] A. I. McIntosh, B. Yang, S. M. Goldup, et al. *Terahertz spectroscopy: a powerful new tool for the chemical sciences?* **Chem. Soc. Rev.** 41.6 (2012), pp. 2072–82. DOI: 10.1039/c1cs15277g.

[23] A. G. Davies, A. D. Burnett, W. Fan, et al. *Terahertz spectroscopy of explosives and drugs*. **Mater. Today** 11.3 (2008), pp. 18–26. DOI: 10.1016/S1369-7021(08)70016-6.

[24] R. S. Krishnan and R. K. Shankar. *Raman Effect: History of the Discovery* (1981), pp. 1–8. DOI: 10.1002/jrs.1250100103.

[25] J. G. Grasselli and B. J. Bulkin. *Analytical Raman spectroscopy*. 1991, p. 461. ISBN: 9780471519553.

[26] L. Ornstein and J Rekveld. *Intensity measurements in the Raman effect and the distribution law of Maxwell-Boltzmann*. **Phys. Rev.** 29 (1929), pp. 720–725. DOI: 10.1103/PhysRev.34.720.

[27] C. L. Zavaleta, M. F. Kircher, and S. S. Gambhir. *Raman's "effect" on molecular imaging*. **J. Nucl. Med.** 52.12 (2011), pp. 1839–44. DOI: 10.2967/jnumed.111.087775.

[28] A. J. Hobro and B. Lendl. *Stand-off Raman spectroscopy*. **Trends Anal. Chem.** 28.11 (2009), pp. 1235–1242. DOI: 10.1016/j.trac.2009.08.008.

[29] J. C. Carter, S. M. Angel, M. Lawrence-Snyder, et al. *Standoff Detection of High Explosive Materials at 50 Meters in Ambient Light Conditions Using a Small Raman Instrument*. **Appl. Spectrosc.** 59.6 (2005), pp. 769–775. DOI: 10.1366/0003702054280612.

[30] J. Moros, J. A. Lorenzo, K. Novotný, et al. *Fundamentals of stand-off Raman scattering spectroscopy for explosive fingerprinting*. **J. Raman Spectrosc.** 44.1 (2013), pp. 121–130. DOI: 10.1002/jrs.4138.

[31] M Gaft and L Nagli. *UV gated Raman spectroscopy for standoff detection of explosives*. **Opt. Mater. (Amst).** 30.11 (2008), pp. 1739–1746. DOI: 10.1016/j.optmat.2007.11.013.

[32] E. L. Izake, S. Sundarajoo, W. Olds, et al. *Standoff Raman spectrometry for the non-invasive detection of explosives precursors in highly fluorescing packaging*. **Talanta** 103.0 (2013), pp. 20–27. DOI: 10.1016/j.talanta.2012.09.055.

[33] A. Pettersson, S. Wallin, H. Östmark, et al. *Explosives standoff detection using Raman spectroscopy: from bulk towards trace detection*. **SPIE 7664, Detect. Sens. Mines, Explos. Objects, Obs. Targets XV, 766401** (2010). DOI: 10.1117/12.852544.

[34] A. K. Misra, S. K. Sharma, T. E. Acosta, et al. *Single-Pulse Standoff Raman Detection of Chemicals from 120 m Distance During Daytime*. **Appl. Spectrosc.** 66.11 (2012), pp. 1279–1285. DOI: 10.1366/12-06617.

[35] D. A. Long. *The Raman Effect: A Unified Treatment of the Theory of Raman Scattering by Molecules*. Chichester, UK: John Wiley & Sons, Ltd, 2002. ISBN: 0471490288. DOI: 10.1002/0470845767.

[36] M. Tanaka and R. J. Young. *Review Polarised Raman spectroscopy for the study of molecular orientation distributions in polymers*. **J. Mater. Sci.** 41.3 (2006), pp. 963–991. DOI: 10.1007/s10853-006-6595-7.

[37] M O'Keefe and N. Brese. *Atom sizes and bond lengths in molecules and crystals*. **J. Am. Chem. Soc.** 12 (1991), pp. 3226–3229. DOI: 10.1021/ja00009a002.

[38] D. J. Griffiths. *Introduction to Electrodynamics*. Prentice Hall, 1999. ISBN: 0139199608.

[39] A. C. Albrecht and M. C. Hutley. *On the Dependence of Vibrational Raman Intensity on the Wavelength of Incident Light*. **J. Chem. Phys.** 55.9 (1971), pp. 4438–4442. DOI: 10.1063/1.1676771.

[40] D. D. Tuschel, A. V. Mikhonin, B. E. Lemoff, et al. *Deep ultraviolet resonance Raman excitation enables explosives detection*. **Appl. Spectrosc.** 64.4 (2010), pp. 425–432. DOI: 10.1366/000370210791114194.

[41] A. Ehlerding, I. Johansson, S. Wallin, et al. *Resonance-Enhanced Raman Spectroscopy on Explosives Vapor at Standoff Distances*. **Int. J. Spectrosc.** 2012 (2012), pp. 1–9. DOI: 10.1155/2012/158715.

[42] J. M. Dudik, C. R. Johnson, and S. A. Asher. *Wavelength Dependence of the Preresonance Raman Cross Sections of CH3CN, SO2-4, ClO-4, and NO-3*. **J. Chem. Phys.** 82.4 (1984), pp. 1732–1740.

[43] S. A. Asher. *UV resonance Raman studies of molecular structure and dynamics: applications in physical and biophysical chemistry*. **Annu. Rev. Phys. Chem.** 39 (1988), pp. 537–88. DOI: 10.1146/annurev.pc.39.100188.002541.

[44] S. A. Asher and C. R. Johnson. *Raman Speciroscopy of Coal Liquid Shows That Fluorescence Interference Is Minimized with Ultraviolet Excitation*. **Science (80-.).** 225.4659 (1984), pp. 311–313. DOI: DOI:10.1126/science.6740313.

[45] *ANSI Z136.1 American National Standard for Safe Use of Lasers*. Laser Institute of America, Orlando, 2007. ISBN: 978-0-912035-65-9.

[46] "IEC/TR 60825-14 Safety of laser products-Part 14: A users guide." 1st ed. 2004.

[47] *AS/NZS IEC 60825.14:2011 Safety of laser products, Part 14, A users guide*. SAI Global Limited/Standards Australia Limited, 2011. ISBN: 978 0 7337 9985 3.

[48] K. Seki, H. Tanaka, T. Ohta, et al. *Electronic Structure of Poly(tetrafluoroethylene) Studied by UPS, VUV Absorption, and Band Calculations*. **Phys. Scr.** 41.1 (1990), pp. 167–171. DOI: 10.1088/0031-8949/41/1/041.

[49] J. Chen, D. Tracy, S. Zheng, et al. *Photoetching and modification of poly(tetrafluoroethylene-co-hexafluoropropylene) polymer surfaces with vacuum UV radiation*. **Polym. Degrad. Stab.** 79.3 (2003), pp. 399–404. DOI: 10.1016/S0141-3910(02)00339-7.

[50] C. K. Manka, S. Nikitin, R. Lunsford, et al. *Wavelength-dependent amplitude of Teflon Raman lines*. **J. Raman Spectrosc.** 42.4 (2011), pp. 685–690. DOI: 10.1002/jrs.2752.

[51] A. K. Misra, S. K. Sharma, D. E. Bates, et al. *Compact standoff Raman system for detection of homemade explosives*. **SPIE 7665, Chem. Biol. Radiol. Nucl. Explos. Sens. XI, 76650U** 7665 (2010), 76650U–76650U–11. DOI: 10.1117/12.849850.

[52] National Consortium for the Study of Terrorism and Responses to Terrorism (START). (2010). *Background Report : On the Fifteenth Anniversary of the Oklahoma City Bombing*. Tech. rep. April 2010. 2010, pp. 1–7.

[53] I. Johansson, E. Ceco, A. Ehlerding, et al. *Stand-off detection of explosives vapors by resonance-enhanced Raman spectroscopy*. **SPIE 8709, Detect. Sens. Mines, Explos. Objects, Obs. Targets XVIII, 87090N** 8709 (2013). Ed. by J. T. Broach and J. C. Isaacs, 87090N–87090N–10. DOI: 10.1117/12.2017858.

Appendix

A.1 MPE Calculations for Common Excitation Wavelengths

Methods for calculating the MPEs in Section 3.1 are found in the AS/NZS IEC 60825.14:2011 standard,[47] with several MPE calculations for common excitation wavelengths shown in this section of the appendix. All calculations are for an excitation laser with a 5 ns pulse duration, a 10 Hz repetition rate, a 1.5 mrad angular subtense, and a 1 second exposure time. From Section 3.1 we see the three requirements for determining the MPE:

a) The exposure from any single pulse within a pulse train shall not exceed the MPE for a single pulse.

b) The average exposure for a pulse train of exposure duration T shall not exceed the MPE for a single pulse of exposure duration T.

c) The average exposure from pulses within a pulse train shall not exceed the MPE for a single pulse multiplied by $N^{-1/4}$.

Where N is the number of pulses expected in an exposure. With condition c) only applicable to ocular exposure from lasers with an excitation wavelength higher than 400 nm and only applicable to individual pulse durations shorter than 0.25 seconds long.

A.1.1 MPE Calculations for 266 nm Excitation

At 266 nm excitation, the standard states that the ocular MPE can be determined to be the lowest of requirements a) and b), as requirement c) does not apply to wavelengths under 400 nm. For requirement a) we must find the exposure from a single pulse in the train of pulses. The standards give this MPE at 266 nm excitation to be 30 J/m^2, giving our MPE for requirement a) to be

$$30 \text{ J/m}^2. \tag{A.1.1}$$

Through requirement b) we must now find the average exposure of a pulse train of exposure T, which is 1 second for our case, and ensure it does not exceed the MPE for a single pulse

of 1 second exposure. The standards show the MPE for a 1 second pulse to also be 30 J/m^2, with a total of 10 pulses in the 1 second exposure from the 10 Hz repetition rate. Therefore, for the total 1 second exposure, the radiant exposure is limited by

$$\frac{30\ J/m^2}{10\ \text{pulses}} = 3\ J/m^2\ \text{per pulse}. \tag{A.1.2}$$

Similarly, for the MPE allowed incident upon skin, the standards give the MPE for requirement a) to be

$$30\ J/m^2. \tag{A.1.3}$$

While the skin's MPE from requirement b) is

$$\frac{30\ J/m^2}{10\ \text{pulses}} = 3\ J/m^2\ \text{per pulse}, \tag{A.1.4}$$

also being the same as the ocular MPE. Clearly the most limiting ocular MPE is from requirement b), while the most limiting skin MPE is also requirement b), both being the same value of 3 J/m^2, giving the best available MPE for 266 nm to be 3 J/m^2.

A.1.2 MPE Calculations for 355 nm Excitation

At 355 nm excitation, the standards state that the ocular MPE can be determined to be the lowest of requirements a) and b), as requirement c) does not apply to wavelengths under 400 nm. For requirement a) we must find the exposure from a single pulse in the train of pulses. The standards give this MPE at 355 nm excitation to be C_1, which is a correction factor given by the standards as

$$C_1 = 5.6 \times 10^3\ t^{0.25}, \tag{A.1.5}$$

where t is the emission duration expressed in seconds. Using our pulse duration of 5 ns, we can calculate C_1 through

$$C_1 = 5.6 \times 10^3 \times (5 \times 10^{-9})^{0.25} \approx 47, \tag{A.1.6}$$

giving our MPE for requirement a) to be approximately

$$47\ J/m^2. \tag{A.1.7}$$

Through requirement b) we must now find the average exposure of a pulse train of exposure T, which is 1 second for our case, and ensure it does not exceed the MPE for a single pulse of 1 second exposure. The standards show the MPE for a 1 second pulse to also be C_1, however our emission duration, t, in our calculation of C_1 is now 1 second, giving a result

of

$$C_1 = 5.6 \times 10^3 \times 1^{0.25} = 5600. \tag{A.1.8}$$

With a total of 10 pulses in the 1 second exposure from the 10 Hz repetition rate, this means that the total 1 second exposure, the radiant exposure is limited by

$$\frac{5600 \text{ J/m}^2}{10 \text{ pulses}} = 560 \text{ J/m}^2 \text{ per pulse.} \tag{A.1.9}$$

Similarly, for the MPE allowed incident upon skin, the standards give the MPE for requirement a) to be C_1, the same as requirement a) from the ocular MPE, while the skin's MPE from requirement b) is the same as requirement b) from the ocular MPE. As the ocular and skin MPEs are the same, it is clear that the most limiting MPE at each is from requirement a), being 47 J/m^2.

A.1.3 MPE Calculations for 532 nm Excitation

At 532 nm excitation, the standards state that the ocular MPE can be determined to be the lowest of requirements a), b), and also requirement c). For requirement a) we must find the exposure from a single pulse in the train of pulses. The standards give this MPE at 532 nm excitation to be

$$5 \times 10^{-3} \; C_6 \text{ J/m}^2, \tag{A.1.10}$$

where C_6 is a correction factor given as:

$$C_6 = \begin{cases} 1 & \text{for } \alpha \leq 1.5 \text{ mrad} \\ \alpha/1.5 \text{ mrad} & \text{for } 1.5 \text{ mrad} < \alpha \leq 100 \text{ mrad} \\ 66.7 & \text{for } \alpha > 100 \text{ mrad} \end{cases}$$

where α is the angular subtense. As our calculations involve a laser with an angular subtense of 1.5 mrad, our C_6 correction factor is simply 1, giving us the ocular MPE for requirement a) as

$$0.005 \text{ J/m}^2. \tag{A.1.11}$$

Similar to the other excitation wavelengths, to obtain the MPE for requirement b) we must now find the average exposure of a pulse train of exposure T, which is 1 second for our case, and ensure it does not exceed the MPE for a single pulse of 1 second exposure. The ocular MPE at 532 nm for a pulse train of 1 second is given by the standards as

$$18 \; t^{0.75} \; C_6 \text{ J/m}^2. \tag{A.1.12}$$

With our emission duration, t, for this requirement being 1 second, and C_6 is 1 as found before, we can find the MPE for the whole duration by

$$18 \times 1^{0.75} \text{ J/m}^2 = 18 \text{ J/m}^2. \tag{A.1.13}$$

With a total of 10 pulses in the 1 second exposure from the 10 Hz repetition rate, this means that over the total 1 second exposure, the radiant exposure is limited by

$$\frac{18 \text{ J/m}^2}{10 \text{ pulses}} = 1.8 \text{ J/m}^2 \text{ per pulse}. \tag{A.1.14}$$

As the excitation wavelength is above 400 nm, requirement c) is now applicable and must be calculated for the ocular MPE. The standards state that the average exposure from pulses in a pulse train must not exceed the MPE of a single pulse multiplied by $\text{N}^{-1/4}$, where N is the number of pulses in the exposure time. For our 1 second exposure, we have our number of pulses, N, equal to 10. Therefore, our ocular MPE from requirement c) is

$$0.005 \text{ J/m}^2 \times 10^{-0.25} \approx 0.0028 \text{ J/m}^2 \text{ per pulse}. \tag{A.1.15}$$

Clearly the most limiting of the ocular MPEs is requirement c), being 0.0028 J/m^2 per pulse. Looking at the skin MPE next, we find that the standards give requirement a) to be

$$200 \text{ J/m}^2. \tag{A.1.16}$$

As requirement b) depends on ensuring that the average exposure of a pulse train of 1 second exposure does not exceed the MPE for a single pulse of 1 second exposure, we first find that the skin MPE at 532 nm for a pulse train of 1 second is given by the standards as

$$1.1 \times 10^4 \ t^{0.25} \text{ J/m}^2. \tag{A.1.17}$$

With a total of 10 pulses in the 1 second exposure from the 10 Hz repetition rate, this means that over the total 1 second exposure, the radiant exposure is limited by

$$\frac{1.1 \times 10^4 \times 1^{0.25} \text{ J/m}^2}{10 \text{ pulses}} = 1100 \text{ J/m}^2 \text{ per pulse}. \tag{A.1.18}$$

As can be seen, the skin MPE requirements a) and b) are much higher than all of the ocular MPE requirements, with the most restrictive MPE being the ocular MPE requirement c) of approximately 0.0028 J/m^2 per pulse.

A.1.4 MPE Calculations for 785 nm Excitation

At 785 nm excitation, the standards state that the ocular MPE can be determined to be the lowest of requirements a), b), and also requirement c). For requirement a) we must

find the exposure from a single pulse in the train of pulses. The standards give this MPE at 785 nm excitation to be

$$5 \times 10^{-3}\ C_4\ C_6\ \text{J/m}^2, \tag{A.1.19}$$

where C_6 is explained in the previous section to be 1, and C_4 is a correction factor given by

$$C_4 = \begin{cases} 10^{0.002(\lambda-700)} & \text{for } 700 \text{ nm} < \lambda \leq 1050 \text{ nm} \\ 5 & \text{for } 1050 \text{ nm} < \lambda \leq 1400 \text{ nm} \end{cases}$$

where λ is the excitation wavelength in nanometres. So for our 785 nm excitation we have a C_4 of

$$C_4 = 10^{0.002(785-700)} \approx 1.48 \tag{A.1.20}$$

Using this correction factor value for C_4 of approximately 1.48 and our C_6 value of 1, we can calculate our ocular MPE for requirement a) by

$$5 \times 10^{-3}\ \times 1.48 \times 1\ \text{J/m}^2 \approx 0.0074\ \text{J/m}^2. \tag{A.1.21}$$

Similar to the other excitation wavelengths, to obtain the MPE for requirement b) we must now find the average exposure of a pulse train of exposure T, which is 1 second for our case, and ensure it does not exceed the MPE for a single pulse of 1 second exposure. The ocular MPE at 785 nm for a pulse train of 1 second is given by the standards as

$$18\ t^{0.75}\ C_4\ C_6\ \text{J/m}^2. \tag{A.1.22}$$

With our emission duration, t, for this requirement being 1 second, C_4 as 1.48, and C_6 is 1 as found before, we can find the MPE for the whole duration by

$$18\ 1^{0.75} \times 1.48\ \text{J/m}^2 \approx 27\ \text{J/m}^2. \tag{A.1.23}$$

With a total of 10 pulses in the 1 second exposure from the 10 Hz repetition rate, this means that over the total 1 second exposure, the radiant exposure is limited by

$$\frac{27\ \text{J/m}^2}{10\ \text{pulses}} = 2.7\ \text{J/m}^2 \text{ per pulse}. \tag{A.1.24}$$

As the excitation wavelength is above 400 nm, requirement c) is now applicable and must be calculated for the ocular MPE. The standards state that the average exposure from pulses in a pulse train must not exceed the MPE of a single pulse multiplied by $\text{N}^{-1/4}$, where N is the number of pulses in the exposure time. For our 1 second exposure, we have our number of pulses, N, equal to 10. Therefore, our ocular MPE from requirement c) is

$$0.0074\ \text{J/m}^2 \times 10^{-0.25} \approx 0.004\ \text{J/m}^2 \text{ per pulse}. \tag{A.1.25}$$

Clearly the most limiting of the ocular MPEs is requirement c), being 0.004 J/m^2 per pulse. Looking at the skin MPE next, we find that the standards give requirement a) to be

$$200 \times C_4 \text{ J/m}^2 \approx 200 \times 1.48 \text{ J/m}^2 \approx 296 \text{ J/m}^2. \tag{A.1.26}$$

As requirement b) depends on ensuring that the average exposure of a pulse train of 1 second exposure does not exceed the MPE for a single pulse of 1 second exposure, we first find that the skin MPE at 785 nm for a pulse train of 1 second is given by the standards as

$$1.1 \times 10^4 \; C_4 \; t^{0.25} \;\; \text{J/m}^2. \tag{A.1.27}$$

With a total of 10 pulses in the 1 second exposure from the 10 Hz repetition rate, this means that over the total 1 second exposure, the radiant exposure is limited by

$$\frac{1.1 \times 10^4 \times 1.48 \times 1^{0.25} \text{ J/m}^2}{10 \text{ pulses}} \approx 1628 \text{ J/m}^2 \text{ per pulse.} \tag{A.1.28}$$

As can be seen, the skin MPE requirements a) and b) are much higher than all of the ocular MPE requirements, with the most restrictive MPE being the ocular MPE requirement c) of approximately 0.004 J/m^2 per pulse.

A.1.5 MPE Calculations for 1064 nm Excitation

At 1064 nm excitation, the standards state that the ocular MPE can be determined to be the lowest of requirements a), b), and also requirement c). For requirement a) we must find the exposure from a single pulse in the train of pulses. The standards give this MPE at 1064 nm excitation to be

$$5 \times 10^{-2} \; C_6 \; C_7 \text{ J/m}^2, \tag{A.1.29}$$

where C_6 is explained in the previous section to be 1, and C_7 is a correction factor equal to 1 between 700 nm and 1150 excitations. Using this correction factor value for C_7 of 1, as well as our C_6 value of 1, we can calculate our ocular MPE for requirement a) at 1064 nm by

$$5 \times 10^{-2} \;\; \times 1 \times 1 \text{ J/m}^2 \approx 0.05 \text{ J/m}^2. \tag{A.1.30}$$

Similar to the other excitation wavelengths, to obtain the MPE for requirement b) we must now find the average exposure of a pulse train of exposure T, which is 1 second for our case, and ensure it does not exceed the MPE for a single pulse of 1 second exposure. The ocular MPE at 1064 nm for a pulse train of 1 second is given by the standards as

$$90 \; t^{0.75} \; C_6 \; C_7 \text{ J/m}^2. \tag{A.1.31}$$

With our emission duration, t, for this requirement being 1 second, C_6 as 1, and C_7 is 1 as found before, we can find the MPE for the whole duration by

$$90 \times 1^{0.75} \times 1 \times 1 \text{ J/m}^2 = 90. \tag{A.1.32}$$

With a total of 10 pulses in the 1 second exposure from the 10 Hz repetition rate, this means that over the total 1 second exposure, the radiant exposure is limited by

$$\frac{90 \text{ J/m}^2}{10 \text{ pulses}} = 9 \text{ J/m}^2 \text{ per pulse.} \tag{A.1.33}$$

As the excitation wavelength is above 400 nm, requirement c) is now applicable and must be calculated for the ocular MPE. The standards state that the average exposure from pulses in a pulse train must not exceed the MPE of a single pulse multiplied by $\text{N}^{-1/4}$, where N is the number of pulses in the exposure time. For our 1 second exposure, we have our number of pulses, N, equal to 10. Therefore, our ocular MPE from requirement c) is

$$0.05 \text{ J/m}^2 \times 10^{-0.25} \approx 0.03 \text{ J/m}^2 \text{ per pulse.} \tag{A.1.34}$$

Clearly the most limiting of the ocular MPEs is requirement c), being 0.03 J/m^2 per pulse. Looking at the skin MPE next, we find that the standards give requirement a) to be

$$200 \times C_4 \text{ J/m}^2, \tag{A.1.35}$$

where C_4 at 1064 nm excitation is equal to 5, as described in the previous section. Using this value of 5 for C_4 we can calculate our skin MPE requirement a) to be

$$200 \times 5 \text{ J/m}^2 = 1000 \text{ J/m}^2. \tag{A.1.36}$$

As requirement b) depends on ensuring that the average exposure of a pulse train of 1 second exposure does not exceed the MPE for a single pulse of 1 second exposure, we first find that the skin MPE at 1064 nm for a pulse train of 1 second is given by the standards as

$$1.1 \times 10^4 \; C_4 \; t^{0.25} \;\; \text{J/m}^2. \tag{A.1.37}$$

With a total of 10 pulses in the 1 second exposure from the 10 Hz repetition rate, this means that over the total 1 second exposure, the radiant exposure is limited by

$$\frac{1.1 \times 10^4 \times 5 \times 1^{0.25} \text{ J/m}^2}{10 \text{ pulses}} = 5500 \text{ J/m}^2 \text{ per pulse.} \tag{A.1.38}$$

As can be seen, the skin MPE requirements a) and b) are much higher than all of the ocular MPE requirements, with the most restrictive MPE being the ocular MPE requirement c) of approximately 0.03 J/m^2 per pulse.

A.2 Aperture Diameters Used to Determine MPE

Spectral Region (nm)	**Aperture diameter for**			
	Eye (mm)			**Skin** (mm)
180 to 400	1			3.5
≥ 400 to 1400	7			3.5
≥ 1400 to 10^5	1 $1.5t^{3/8}$ 3.5	for for for	$t \leq 0.35$ s 0.35 s < t < 10 s $t \geq 10$ s	3.5
≥ 10^5 to 10^6	11			11

Aperture diameters used for the development of Figure 3.5 from Section 3.1.[47]

A.3 Quantum Efficiency of the PI-MAX4 ICCD Camera

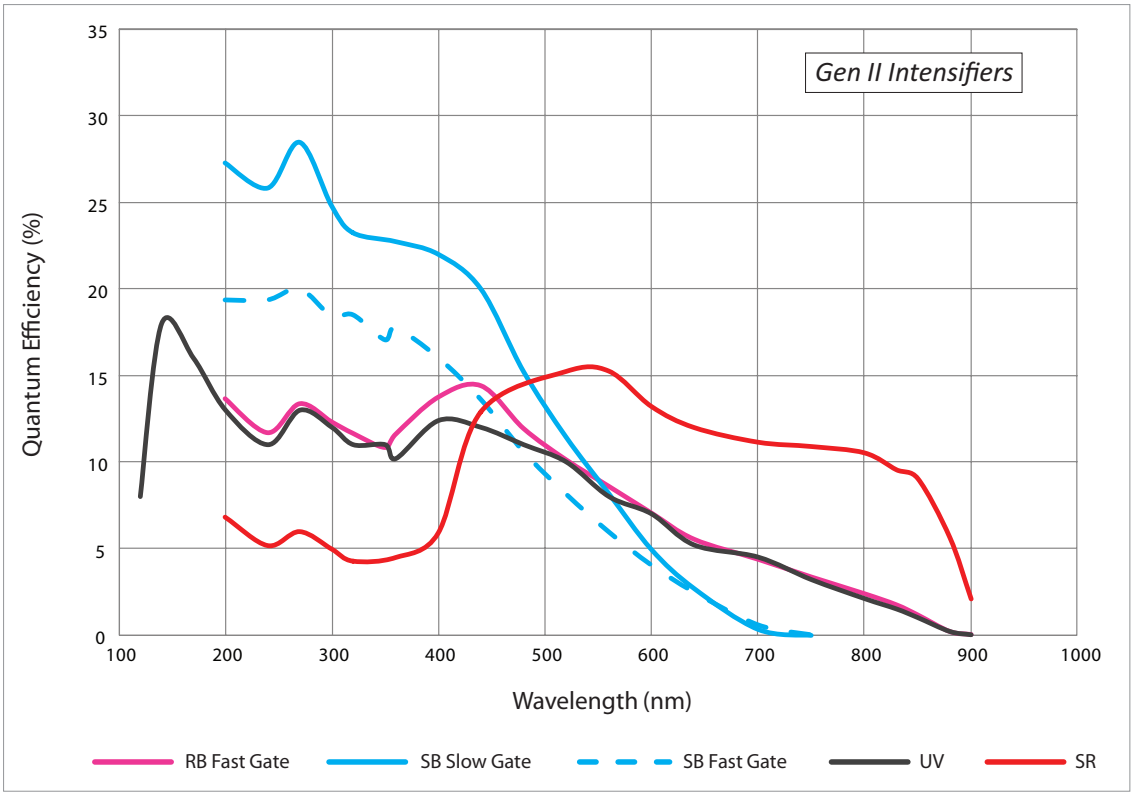

Quantum efficiency of the PI-MAX4 camera. The camera used had a SR intensifier (shown in red). Image obtained from Princeton Instruments at:
http://www.princetoninstruments.com/Uploads/Princeton/Documents/Datasheets/PIMAX4/Princeton_Instruments_PI-MAX4_1024x256_rev_N3_1-23-14.pdf

A.4 Quantum Efficiency for the UV Diffraction Grating

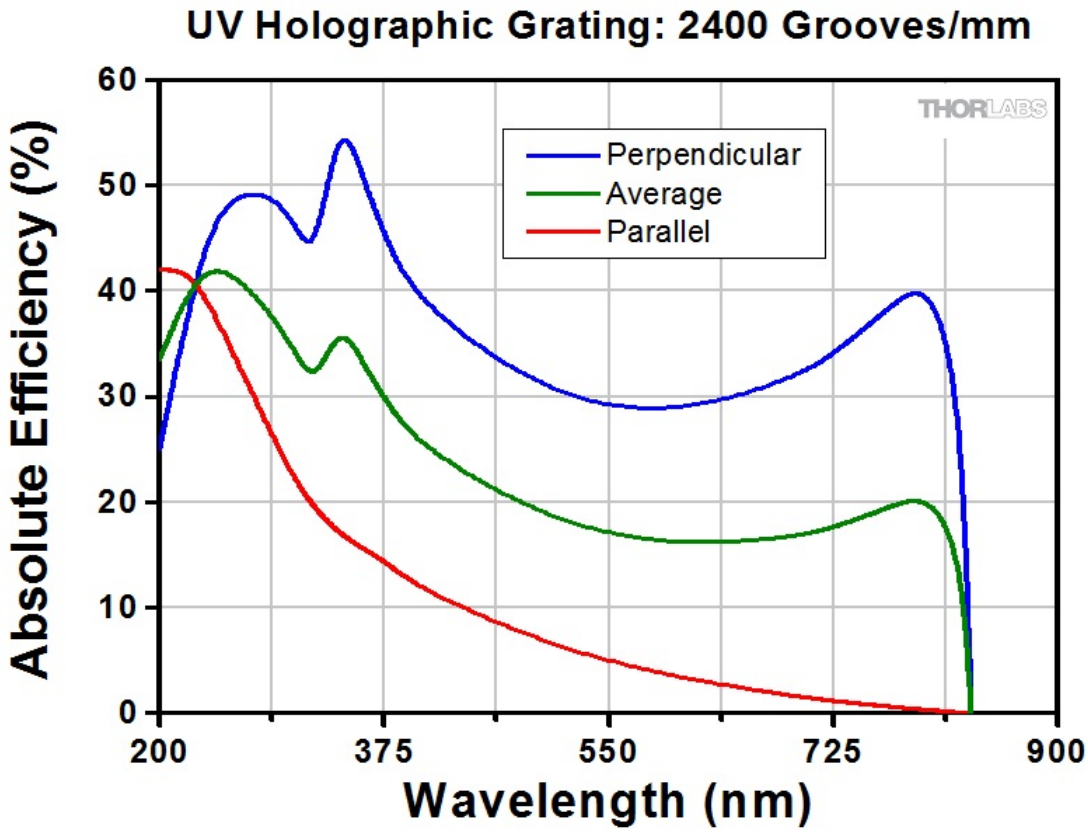

Quantum efficiency of the UV diffraction grating. Image obtained from Thorlabs at: http://www.thorlabs.com/images/tabImages/Grating_Eff_Holo_UV2400_G1-780.gif

A.5 Quantum Efficiency of the Visible Diffraction Grating

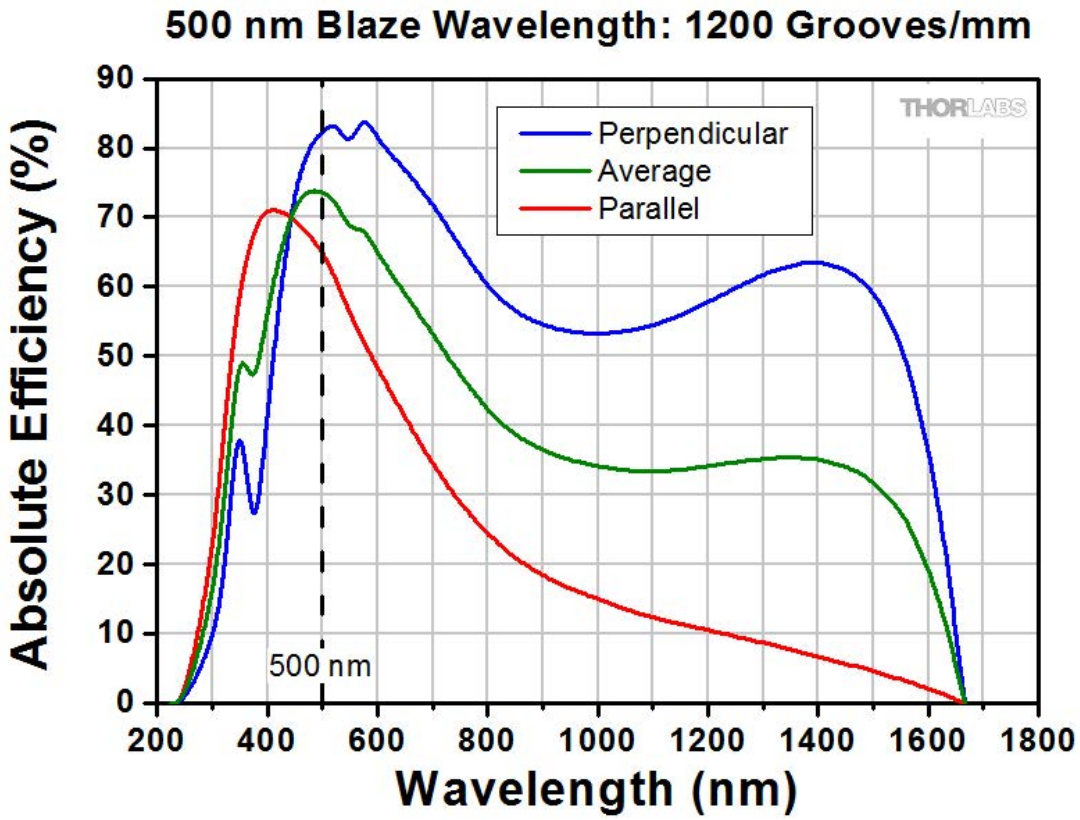

Quantum efficiency of the visible diffraction grating. Image obtained from Thorlabs at: http://www.thorlabs.com/images/tabImages/500_1200_Ruled_Grating_Efficiency_Graph_780.gif

A.6 Quantum Efficiency of the UV Edge Filter

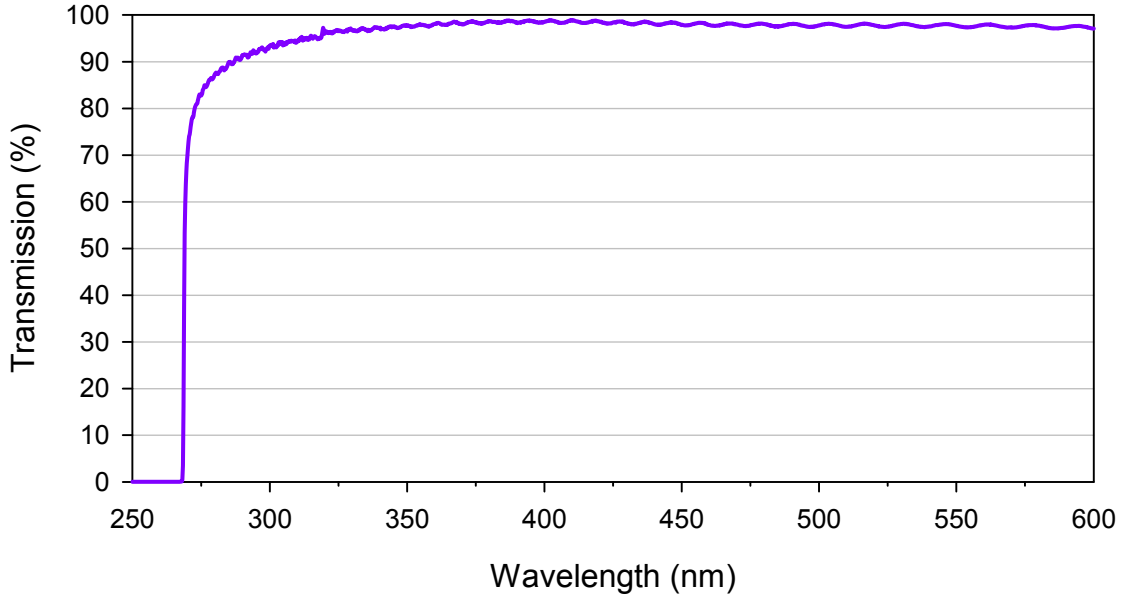

Quantum efficiency of the UV edge filter. (Semrock 266 nm RazorEdge ultrasteep long-pass edge filter)

A.7 Quantum Efficiency of the Visible Edge Filter

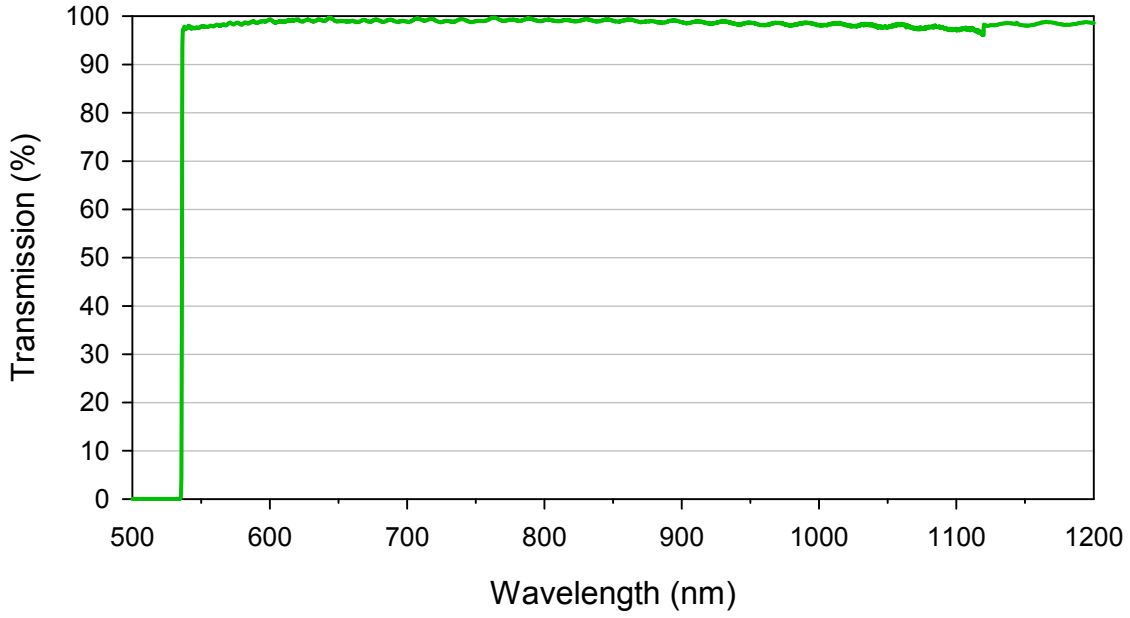

Quantum efficiency of the visible edge filter. (Semrock 532 nm RazorEdge ultrasteep long-pass edge filter)